Biophysical Chemistry 197 (2015) 25–39

Contents lists available at ScienceDirect

Biophysical Chemistry

journal homepage: http://www.elsevier.com/locate/biophyschem

Site-directed mutagenesis of rat α-parvalbumin: replacement of canonical CD-site residues with their non-consensus counterparts from rat β-parvalbumin

Michael T. Henzl *, Arthur G. Sirianni, Lindsey A. Markus, Christine M. Davis

Department of Biochemistry, University of Missouri, Columbia, MO, USA 65211

HIGHLIGHTS

- Residues 49, 50, 57–60 were replaced with their counterparts from rat β-parvalbumin.
- E59D, alone or with the other mutations, confers Ca^{2+}-specificity on the CD site.
- In contrast to the CD site, EF-site affinity is not compromised by the mutations.
- The consequences of replacing L85 with phenylalanine were also examined.
- L85F improves Ca^{2+} affinity in wild-type rat α but has little impact in the variants.

GRAPHICAL ABSTRACT

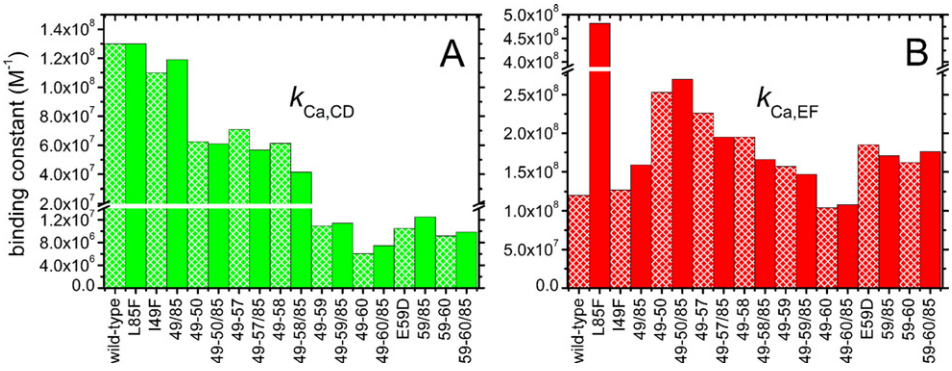

ARTICLE INFO

Article history:
Received 15 September 2014
Received in revised form 2 December 2014
Accepted 3 December 2014
Available online 11 December 2014

Keywords:
Ca^{2+}-binding proteins
EF-hand proteins
Parvalbumin
Oncomodulin
ITC
DSC

ABSTRACT

Rat β-parvalbumin (β-PV) displays low divalent-ion affinity. Its CD site is distinguished by six non-consensus residues – the "CD-loop residues" – at positions 49, 50, 57–60. Additionally, leucine occupies position 85, rather than phenylalanine, the β-lineage-consensus residue. Replacement of the CD-loop residues in rat β with the canonical residues was previously found to have little effect on divalent-ion affinity, unless L85 is replaced by phenylalanine. Herein, we replace the canonical CD-loop residues in rat α-PV with their rat β-PV counterparts. Although the mutations have a generally modest impact on affinity, E59D confers Ca^{2+}-specificity on the CD site, in the presence or absence of the other mutations. Despite their minimal impact on ΔG, several CD-loop mutations markedly alter ΔH, evidently by perturbing the apo-protein conformation. The L85F mutation was also examined. In wild-type rat α, L85F increases EF-site Ca^{2+} affinity. In the CD-loop variants, the mutation leaves the ΔG for Ca^{2+}-binding largely unaffected. However, several variants display highly exothermic binding enthalpies, indicative of ligation-linked protein-folding. Consistent with that idea, scanning-calorimetry data confirm that L85F has significantly destabilized those proteins.

The vast majority of intracellular Ca^{2+}-binding proteins belong to the EF-hand family [1–4]. The 242 family members encoded by the human genome are participants in Ca^{2+}-signaling pathways, functioning either as Ca^{2+}-dependent regulatory proteins or cytosolic Ca^{2+} buffers. The hallmark of the EF-hand family is its distinctive divalent-ion-binding motif, a highly conserved central ion-binding loop flanked

* Corresponding author at: Department of Biochemistry, 117 Schweitzer Hall, University of Missouri, Columbia, MO 65211. Tel.: +1 573 882 7485; fax: +1 573 884 4812.
E-mail address: henzlm@missouri.edu (M.T. Henzl).

http://dx.doi.org/10.1016/j.bpc.2014.12.002
0301-4622/

by short amphipathic helices. The spatial arrangement of these structural elements, which can be mimicked with the thumb and first two fingers of the right hand, inspired the term "EF-hand" [5].

In the classical EF-hand motif, the ligands to the bound metal ion are arrayed at the approximate vertices of an octahedron and are indexed by Cartesian axes ($x, y, z, -y, -x, -z$). A main-chain carbonyl furnishes the $-y$ ligand; a water molecule commonly resides at $-x$; and a glutamyl side-chain occupies the $-z$ position. The remaining ligands are contributed by side-chain oxygen atoms, most commonly aspartyl carboxylates. Because the $-z$ glutamate binds Ca^{2+}, but not Mg^{2+}, in a bidentate manner, the Ca^{2+}-coordination geometry is actually pentagonal bipyramidyl.

EF-hand proteins exhibit large variations in divalent ion affinity, despite the similarity of their metal ion-binding sites. Elucidation of the physical basis for these differences could enhance our understanding of EF-hand-protein-function specifically and protein-ligand interactions in general. The parvalbumins [6–8] offer a useful model system for examining this issue. These small ($M_r \approx 12{,}000$), vertebrate-specific proteins, which function primarily as Ca^{2+} buffers, contain two EF-hand motifs. The parvalbumin (PV) tertiary structure includes six helices (A-F), organized into two domains (Fig. 1). The Ca^{2+}-binding domain (or CD-EF domain) encompasses two EF-hand motifs, the CD and EF sites, named for the helical elements flanking the binding loops. The N-terminal AB domain, consisting of residues 1–38, packs tightly against the hydrophobic aspect of the CD-EF domain.

Parvalbumins can be assigned to α- and β-lineages on the basis of isoelectric point (pI < 5 for β isoforms), several lineage-specific sequence differences, and the length of the C-terminal helix (one residue longer in α isoforms). Mammals express one α-PV and one β-PV [9]. The α isoform is believed to function as a mobile cytosolic Ca^{2+} buffer in select neurons and muscle fibers. The physiological role of the β isoform (a.k.a. oncomodulin) is less certain. It is abundant in the outer-hair-cells of the cochlea [10] and is also expressed in, and secreted by, macrophages. The secreted protein exhibits potent nerve-growth activity [11].

Although the peptide backbones of the rat α- and β-parvalbumins are nearly superimposable, with an average RMSD of just 0.8 Å, the α isoform exhibits superior divalent ion affinity. In saline at pH 7.4, the overall standard free energies for Ca^{2+} binding differ by 3.5 kcal mol^{-1}; when K^+ replaces Na^+ as the major solvent-cation, the difference increases to 5.5 kcal mol^{-1} [12].

The striking similarity of the bound proteins suggested that the disparity in divalent-ion affinities might reflect structural differences in the Ca^{2+}-free forms. Consistent with this idea, the conformations of Ca^{2+}-free and -bound rat α-PV are very similar [13], whereas those of the rat β isoform are substantially different [14]. In the latter, Ca^{2+} binding is accompanied by reorientation of the C, D, and E helices and reorganization of the hydrophobic core. Conceivably, the energetic cost of this rearrangement is responsible for the attenuated divalent-ion affinity.

Within the CD site (residues 41–70), the sequence of rat β-PV exhibits six departures from the highly conserved PV consensus (Fig. 2). Two of these, F49 and I50, reside at the N-terminal boundary of the binding loop; the remaining four – Y57, L58, D59, and G60 – reside within the loop itself. For convenience, the six residues will be referred to collectively as the "CD-loop residues". Beyond the CD-site borders, the rat β-PV sequence exhibits another anomaly – the presence of leucine rather than phenylalanine, the consensus β-lineage residue, at position 85. Although the uniqueness of the CD-loop sequence eccentricities implies functional significance, replacement with the consensus residues at all six positions provides only a small improvement in the standard binding free energy [15], 0.5 kcal mol^{-1}. Interestingly, however, if L85 is also replaced by phenylalanine, Ca^{2+} affinity increases by 2.3 kcal mol^{-1}, relative to the wild-type β isoform [16]. Mutation of L85 alone improves Ca^{2+} affinity by 1.0 kcal mol^{-1}. Thus, residues 49, 50, 57, 58, 59, 60, and 85 significantly influence divalent ion affinity in rat β-PV, and they act cooperatively.

The generality of these findings is a matter of some interest. To address that question, we have examined the impact of replacing the CD-loop residues in rat α-PV with the non-consensus residues found in the rat β isoform. We have also ascertained the consequences of replacing L85 in each of the variant proteins with phenylalanine. In each case, the divalent ion-binding behavior was examined by isothermal titration calorimetry (ITC).

1. Materials and methods

1.1. Materials

Hepes, NaCl, NaH_2PO_4, $CaCl_2 \cdot 2H_2O$, $MgCl_2 \cdot 2H_2O$, and $Na_2EDTA \cdot 2H_2O$, were purchased from Fisher Scientific Co. EGTA, NTA, tris-hydroxypropyl phosphine (THP) and dipalmitoylphosphatidylcholine (DPPC) were purchased from Sigma-Aldrich. All other chemicals and reagents were obtained from Fisher.

1.2. Protein mutagenesis, expression, and purification

Prior to the study, the coding sequences for the rat α and β isoforms had been cloned into pBluescript. When *Escherichia coli* DH5α is the host strain, the proteins are expressed constitutively at high levels.

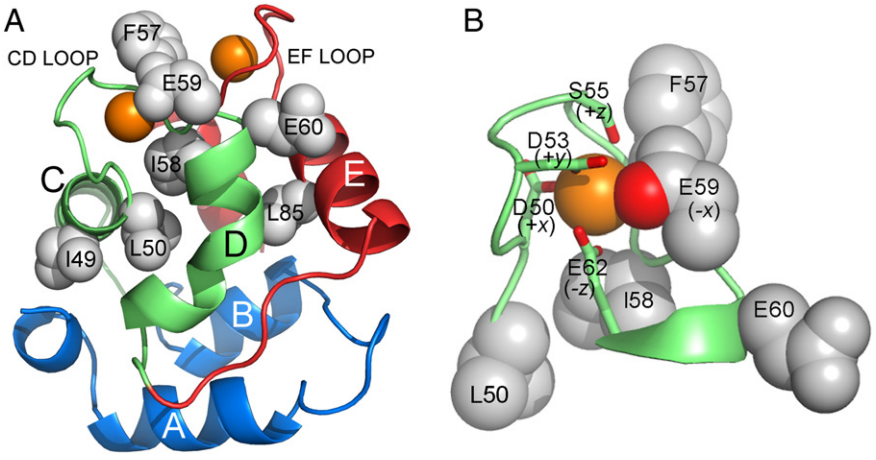

Fig. 1. Rat α-parvalbumin (A) Parvalbumin tertiary structure. (PDB 1RWY). The AB domain is rendered in blue, the CD site in green, and the EF site in red/orange. The bound Ca^{2+} ions are colored orange. The side-chains of the residues subjected to mutagenesis in this work are displayed in space-filling format. (B) A close-up of the CD-site binding loop, emphasizing the coordination of the Ca^{2+}. The *-y* ligand, a main-chain carbonyl contributed by F57, is hidden in this view. This figure and the structures in Fig. 11 were produced with Pymol.

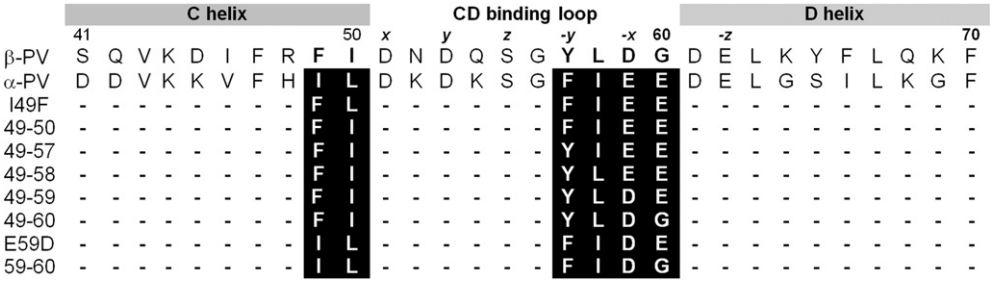

Fig. 2. Comparison of the α- and β-PV sequences within the CD site. The β-PV CD-site harbors six sequence anomalies (highlighted in boldface type). Given that even single-residue departures from the parvalbumin consensus, represented by the residues in the α-PV sequence, are rare at these positions, the mammalian β-PV is highly idiosyncratic.

Purifications typically begin with cell paste collected from two 1-L stationary-phase cultures.

Mutations were made with the Quik-Change mutagenesis kit (Agilent), using custom oligonucleotides produced by Integrated DNA Technologies (Coralville, IA). In every case, the fidelity of the resulting sequence was verified by automated DNA sequencing.

Several of the α-PV variants display diminished affinity for DEAE-Sepharose, even in the divalent ion-free state at very low ionic strength, necessitating a modification of the standard purification protocol [17]. The bacterial cell paste was suspended in five volumes of 20 mM Hepes, pH 7.4, treated with lysozyme, and extruded from a French pressure cell. The resulting lysate (containing 1 mM Ca^{2+}, 10 mM Mg^{2+}, and 2 mM THP) was rapidly heated to 80 °C, maintained there for 5 min, rapidly cooled to 4 °C in an ice-water bath, and clarified by centrifugation. The supernatant was passed over a 15-mL column of DEAE-Sepharose (pre-equilibrated with 20 mM Hepes), followed by 20 mL of buffer. The eluate was then dialyzed for 36 h against 4 L of deionized water at 4 °C. After adding EDTA (to 1 mM), the solution was loaded onto 15 mL of DEAE-Sepharose that had been extensively washed with water. Elution was performed with a linear Ca^{2+} gradient (0–50 mM, 100 mL total volume) prepared in 1 mM Hepes, pH 7.4. Fractions containing the protein of interest were combined, concentrated to 5.0 mL, and loaded onto a Sephadex G-75 column (2.5 × 75 cm). The purity of the resulting protein exceeded 98% in all cases, as judged by SDS-PAGE. For variants harboring the F57Y mutation, protein concentrations were estimated at 274 nm, assuming $\varepsilon_{274} = 1400\ M^{-1}\ cm^{-1}$. Otherwise, the absorbance at 258 nm was used for quantitation, assuming $\varepsilon_{258} = 1600\ M^{-1}\ cm^{-1}$, $1800\ M^{-1}\ cm^{-1}$ (if the protein also harbored the I49F or L85F mutation), or $2000\ M^{-1}\ cm^{-1}$ (if both I49F and L85F were present).

Purification of the D59E and D59E/L85F variants of rat β-parvalbumin was achieved with the standard protocol [18]. Concentrations were estimated spectrophotometrically, assuming $\varepsilon_{274} = 2970\ M^{-1}\ cm^{-1}$.

Isothermal Titration Calorimetry measurements were conducted in a MicroCal VP-ITC (Malvern Instruments, Inc.). Although nearly all of the experiments were conducted at 25 °C, several of the proteins were also titrated with Ca^{2+} at 5 °C, to obtain estimates of the heat-capacity change associated with Ca^{2+} binding. Prior to ITC analysis, Ca^{2+} was removed from the protein preparations by passage over EDTA-agarose [19,20]. The residual Ca^{2+} content was less than 0.02 molar-equivalents in every case, as measured by flame-atomic-absorption at 422.7 nm. The Ca^{2+}-free protein samples were subjected to a battery of titrations.

As in the previous study of rat β-PV, these included titrations with Ca^{2+} in the absence and presence of Mg^{2+} or competitive chelators (EDTA, EGTA, NTA) and with Mg^{2+} in the absence and presence of EDTA. In certain cases, samples were also simultaneously titrated with Ca^{2+} and Mg^{2+} [21]. A 2 μL pre-injection was included at the start of each experiment, the heat from which was neglected during the fitting process. Raw data were integrated with the software supplied with the instrument, and the resulting composite data set was analyzed by global least-squares minimization, to obtain the binding constants and enthalpies for Ca^{2+} and Mg^{2+}. The binding models employed in the analysis incorporated microscopic, or site-specific, binding constants. The binding constants associated with the Ca^{2+}- and Mg^{2+}-binding events at the CD site are denoted $k_{Ca,CD}$ and $k_{Mg,CD}$, and the accompanying enthalpy changes are denoted by $\Delta H_{Ca,CD}$ and $\Delta H_{Mg,CD}$. The corresponding EF-site binding parameters are denoted $k_{Ca,EF}$, $k_{Mg,EF}$, $\Delta H_{Ca,EF}$, and $\Delta H_{Mg,EF}$.

Each iteration of the least-squares analysis requires estimation of the free Ca^{2+} and/or Mg^{2+} concentration(s). For example, to obtain the free Ca^{2+} concentration, $[Ca^{2+}]$, at a given point in a titration, we define a function *FC* representing the difference between the actual and calculated values of the total metal ion concentration:

$$FC = \left[Ca^{2+}\right] + [PV]_t\left[\frac{k_{Ca,EF}\left[Ca^{2+}\right]}{1 + k_{Ca,EF}\left[Ca^{2+}\right]} + \frac{k_{Ca,CD}\left[Ca^{2+}\right]}{1 + k_{Ca,CD}\left[Ca^{2+}\right]}\right] - \left[Ca^{2+}\right]_t \tag{1}$$

In this equation, $[Ca^{2+}]_t$ and $[PV]_t$ represent the actual total Ca^{2+} and protein concentrations. The central term on the right-hand side represents the calculated bound Ca^{2+} concentration, obtained using the current estimates of the binding constants. The value of $[Ca^{2+}]$ is varied to minimize *FC*.

If a small-molecule chelator is present – e.g., EGTA – the *FC* function includes a term representing the metal-ion bound to the chelator:

$$FC = \left[Ca^{2+}\right] + [EGTA]_t\left[\frac{K_{EGTA}\left[Ca^{2+}\right]}{1 + K_{EGTA}\left[Ca^{2+}\right]}\right] + [PV]_t\left[\frac{k_{Ca,EF}\left[Ca^{2+}\right]}{1 + k_{Ca,EF}\left[Ca^{2+}\right]} + \frac{k_{Ca,CD}\left[Ca^{2+}\right]}{1 + k_{Ca,CD}\left[Ca^{2+}\right]}\right] - \left[Ca^{2+}\right]_t \tag{2}$$

where $[EGTA]_t$ is the total EGTA concentration, and K_{EGTA} is the Ca^{2+}-binding constant for EGTA.

Finally, for titrations with Ca^{2+} in the presence of Mg^{2+}, it is necessary to solve the following two equations simultaneously for $[Ca^{2+}]$ and $[Mg^{2+}]$:

$$FC = \left[Ca^{2+}\right] + [PV]_t\left[\frac{\frac{k_{Ca,EF}\left[Ca^{2+}\right]}{1 + k_{Ca,EF}\left[Ca^{2+}\right] + k_{Mg,EF}\left[Mg^{2+}\right]} + \frac{k_{Ca,CD}\left[Ca^{2+}\right]}{1 + k_{Ca,CD}\left[Ca^{2+}\right] + k_{Mg,CD}\left[Mg^{2+}\right]}}\right] - \left[Ca^{2+}\right]_t \tag{3}$$

$$FM = \left[Mg^{2+}\right] + [PV]_t \left[\frac{\frac{k_{Mg,EF}\left[Mg^{2+}\right]}{1 + k_{Ca,EF}\left[Ca^{2+}\right] + k_{Mg,EF}\left[Mg^{2+}\right]} + \frac{k_{Mg,CD}\left[Mg^{2+}\right]}{1 + k_{Ca,CD}\left[Ca^{2+}\right] + k_{Mg,CD}\left[Mg^{2+}\right]}} \right] - \left[Mg^{2+}\right]_t \quad (4)$$

After estimating the free metal-ion concentration(s), one then calculates the cumulative heat of binding. For titrations with Ca^{2+} in the presence of Mg^{2+},

$$Q_i = V_o[PV]_t \left[\frac{\frac{\Delta H_{Ca,EF} k_{Ca,EF}\left[Ca^{2+}\right] + \Delta H_{Mg,EF} k_{Mg,EF}\left[Mg^{2+}\right]}{1 + k_{Ca,EF}\left[Ca^{2+}\right] + k_{Mg,EF}\left[Mg^{2+}\right]} + \frac{\Delta H_{Ca,CD} k_{Ca,CD}\left[Ca^{2+}\right] + \Delta H_{Mg,CD} k_{Mg,CD}\left[Mg^{2+}\right]}{1 + k_{Ca,CD}\left[Ca^{2+}\right] + k_{Mg,CD}\left[Mg^{2+}\right]}} \right] \quad (5)$$

Here Q_i represents the cumulative heat after the i^{th} injection, and V_o is the sample-cell volume. Lastly, an estimate for the injection heat is obtained by calculating the difference between the cumulative heats associated with the *i* and *i-1* data points, including a correction for the volume of reaction mixture displaced by the i^{th} injection (dV):

$$q_i = Q_i - Q_{i-1} + \left(\frac{dV}{V_o}\right)\frac{Q_i + Q_{i-1}}{2} \quad (6)$$

The data treatment has been described in greater detail elsewhere [20,22].

The analysis employed these previous [22] estimates for the Ca^{2+}-binding constants of EDTA, EGTA, and NTA in Hepes-buffered saline, pH 7.4: 4.4×10^7, 1.7×10^7, and 1.10×10^4 M^{-1}, respectively. The corresponding enthalpies were −6.30, −7.80, and −1.96 kcal mol^{-1}. The Mg^{2+}-binding parameters for EDTA were assumed to be 5.50×10^5 M^{-1} and 4.25 kcal mol^{-1}.

1.3. Differential scanning calorimetry (DSC)

Several of the α-PV variants were examined by DSC, employing a modified Nano-DSC instrument (Calorimetry Sciences Corp.), equipped with cylindrical Hastalloy cells (0.32 mL active volume). Temperature-calibration was verified with DPPC, and internally-generated electrical-calibration pulses were used to confirm the accuracy of the differential-power measurements.

Prior to analysis, the proteins were dialyzed extensively against phosphate-buffered saline (PBS), pH 7.4, containing 1.0 mM EDTA. The samples, at concentrations between 4.0 and 6.0 mg/mL, were placed under vacuum for five minutes to remove dissolved gases, then loaded into the sample cell. The reference cell was filled with an aliquot of the dialysis buffer. A scan-rate of 1 K min^{-1} was used for the analyses. All of the samples denatured reversibly, exhibiting an exotherm on cooling and an endotherm on rescan.

Data-analysis was performed with the CpCalc software supplied with the calorimeter. A baseline scan, collected with both cells filled with buffer, was subtracted from the protein-scan prior to analysis. After conversion to molar heat capacity, a transition baseline was subtracted from the data – employing linear- and quadratic fits to the pre- and post-transition regions of the scan, respectively. The resulting excess-heat-capacity data were treated with a two-state denaturation model, to obtain estimates for the melting temperature and van't Hoff enthalpy.

2. Results

This laboratory has had a long-standing interest in the disparate divalent-ion-binding affinities of the mammalian α- and β-PV isoforms. We herein explore the consequences of successively replacing I49, L50, F57, I58, E59, and E60 in the CD site of rat α-PV with the corresponding residues in rat β-PV. Additionally, we examine the E59D and E59D/E60G variants. As shown in Fig. 2, whereas F57, I58, E59, and E60 reside within the 12-residue binding loop – at positions 7, 8, 9, and 10, respectively – I49 and L50 reside at the N-terminal boundary. However, all six are herein referred to collectively as the CD-loop residues.

For brevity, a shorthand notation has been employed to designate variant proteins harboring multiple mutations. For example, α 49–58 denotes the protein in which the β-PV residue has been introduced at positions 49, 50, 57, and 58 – i.e., I49F/L50I/F57Y/L58I. For reference, the abbreviations for each of the multiple-site variant are displayed in Fig. 3.

This study mirrors an earlier one performed on the rat β isoform, in which the aforementioned CD-loop residues were replaced with the canonical rat α residues [16]. In that study, residue 85 – residing outside the CD site *per se* – was identified as a critical determinant of divalent ion-binding affinity. Accordingly, we have also assessed the impact of replacing L85 with phenylalanine in the α-PV CD-loop variant proteins. Finally, we have conducted a detailed characterization of the D59E and D59E/L85F variants of rat β-PV, which had been omitted in the previous β-PV study.

The divalent-ion-binding signature of each protein was assessed by global analysis of multiple ITC experiments, employing an independent two-site model to extract estimates for the Ca^{2+}- and Mg^{2+}-binding constants and -enthalpies. In every case, the model afforded a satisfactory fit to the integrated ITC data. A representative analysis, for the α 49–60 variant, is displayed in Fig. 4.

The binding-parameter estimates for each protein included in the study are listed in Table 1. It should be noted that the Ca^{2+}-binding properties of α E59D and β D59E have been discussed in an earlier publication [23]. Additionally, the divalent-ion-binding parameters for α-PV 49–60/85 have been reported previously [21].

For the two β-PV variants, alignment of the values with the CD- or EF site was straightforward because the former has much lower intrinsic divalent-ion affinity. However, the rationale for assigning the α-PV values deserves comment. Although the CD- and EF sites in wild-type rat α exhibit nearly identical divalent-ion affinities, the associated binding enthalpies differ. The assignment of the wild-type enthalpies exploited the monovalent-ion-binding properties of the protein. Whereas rat α-PV displays no measurable affinity for K^+, it binds a single equivalent of Na^+, with $K_{Na} = 630 \pm 130$ M^{-1} in hepes-buffered saline [24]. The Na^+-binding event – which reduces apparent divalent-ion affinity by an order of magnitude – was attributed to the CD site, based on the alterations in the ^1H-^{15}N-HSQC spectrum that occurred when the major solvent cation was switched from K^+ to Na^+ [24]. It was reasoned, in turn, that the CD-site-binding parameters should exhibit the greater sensitivity to solvent cation identity. Thus, in the analysis of the wild-type α-PV calorimetric data, the microscopic Ca^{2+}- and Mg^{2+}-binding

Abbreviation	Mutations
α 49-50	I49F+L50I
α 49-50/85	I49F+L50I+L85F
α 49-57	I49F+L50I+Y57F
α 49-57/85	I49F+L50I+Y57F+L85F
α 49-58	I49F+L50I+Y57F+I58L
α 49-58/85	I49F+L50I+Y57F+I58L+L85F
α 49-59	I49F+L50I+Y57F+I58L+E59D
α 49-59/85	I49F+L50I+Y57F+I58L+E59D+L85F
α 49-60	I49F+L50I+Y57F+I58L+E59D+E60G
α 49-60/85	I49F+L50I+Y57F+I58L+E59D+E60G+L85F
α 59-60	E59D+E60G
α 59-60/85	E59D+E60G+L85F

Fig. 3. Shorthand nomenclature used to denote the multi-site variant proteins examined in this work.

constants displaying the greater changes in binding enthalpy upon solvent-cation exchange were assigned to the CD site.

As for the variant proteins, binding constants were assigned with the assumption that mutations should perturb the proximal binding site more strongly. In general, the assignments were straightforward, although α I49F presented a challenge. In that case, the two Ca^{2+} binding constants were similar, comparable to the wild-type values. However, the Mg^{2+} values differed appreciably. Thus, the smaller was assigned to the CD site, along with the associated Ca^{2+} constant, consistent with the idea that the mutation should have a greater local impact.

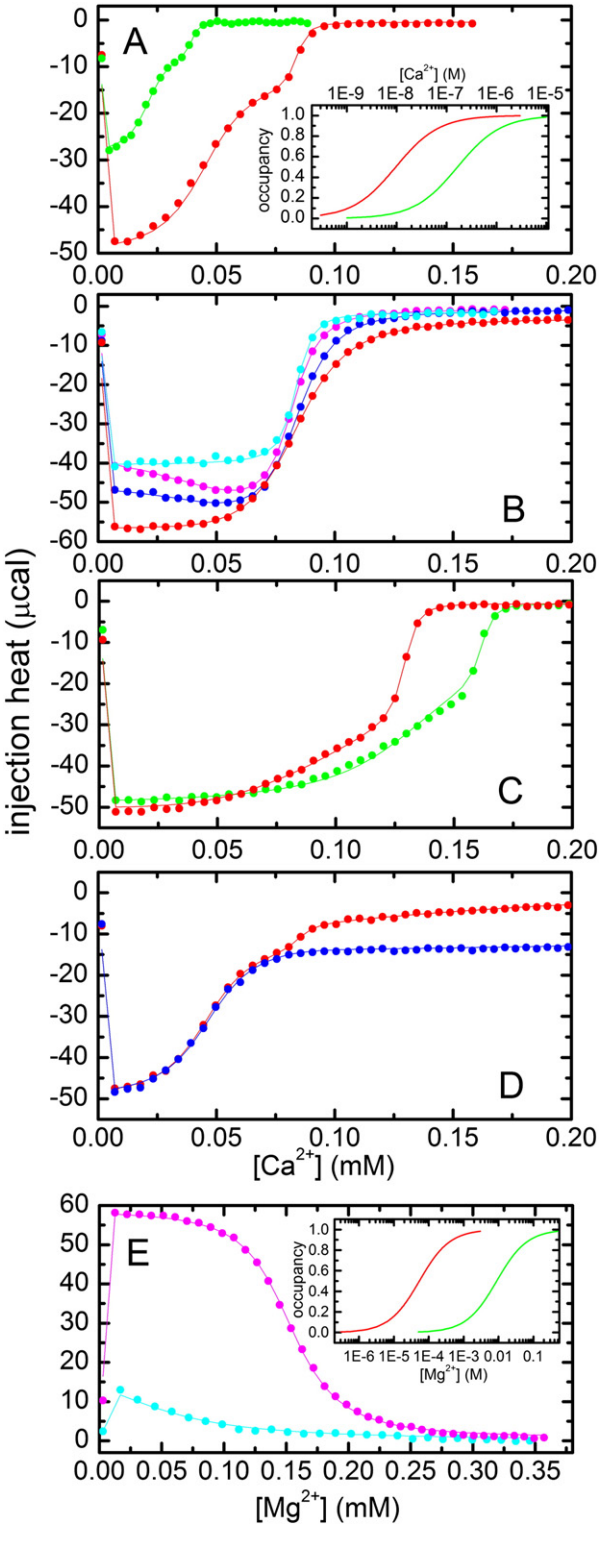

2.1. Binding constants: CD-loop variants

The binding constants for each of the α-PV CD-loop variants are represented by the cross-hatched columns in Fig. 5. In wild-type α, $k_{Ca,CD}$ is $1.3 \times 10^8\ M^{-1}$. As the CD-loop mutations are introduced, the CD-site Ca^{2+} affinity decreases in two major steps (Fig. 5A). I49F alone has little effect, but introduction of L50I, to produce α 49–50, drops $k_{Ca,CD}$ to $6.23 \times 10^7\ M^{-1}$. Although the subsequent F57Y and I58L mutations have little impact on that value, replacement of E59 by aspartate in the α 49–58 background shrinks $k_{Ca,CD}$ to $1.09 \times 10^7\ M^{-1}$. Introduction of E60G mutation into α 49–59 produces further attenuation, to $6.03 \times 10^6\ M^{-1}$.

In wild-type α, $k_{Mg,CD}$ has a value of $2.05 \times 10^4\ M^{-1}$. The CD-site Mg^{2+} affinities of the CD-loop variants (cross-hatched columns in Fig. 5C) roughly parallel the Ca^{2+} affinities, although the I49F and I58L mutations produce more prominent reductions in affinity. As observed for $k_{Ca,CD}$, the E59D mutation has the greatest impact on $k_{Mg,CD}$, reducing it from 3.44×10^3 in α 49–58 to $96\ M^{-1}$. Subsequent replacement of E60 by glycine produces no further attenuation of CD-site Mg^{2+} affinity. In fact, $k_{Mg,CD}$ increases marginally to $113\ M^{-1}$.

Significantly, replacement of E59 by aspartate has virtually the same impact in the wild-type and α 49–58 backgrounds. The $k_{Ca,CD}$ and $k_{Mg,CD}$ values measured for α E59D are 1.05×10^7 and $99\ M^{-1}$, respectively. The corresponding values obtained for the α 49–59 variant are 1.09×10^7 and $96\ M^{-1}$.

In contrast to the CD-site behavior, the CD-loop mutations do not lower EF-site divalent-ion affinity (cross-hatched columns in Fig. 5B and D). In each of the CD-loop variants, $k_{Mg,EF}$ exceeds the wild-type value of $1.61 \times 10^4\ M^{-1}$, and in several of the proteins, the increase in affinity is substantial. For example, α 49–50, α 49–57, and α 49–58 exhibit $k_{Mg,EF}$ values of 4.98×10^4, 3.03×10^4, and $3.26 \times 10^4\ M^{-1}$, respectively. Similarly, with the exception of α 49–60, the EF-site Ca^{2+}-binding constants likewise exceed the wild-type value ($1.20 \times 10^8\ M^{-1}$). The $k_{Ca,EF}$ values of α 49–50, α 49–57, and α 49–58 are particularly noteworthy – 2.53×10^8, 2.26×10^8, and $1.95 \times 10^8\ M^{-1}$, respectively.

2.2. Binding constants: L85F variants

Because the identity of residue 85 (whether leucine or phenylalanine) has a major impact on the divalent-ion-binding signatures of the CD-loop variants in rat β-PV, the consequences of the L85F mutation were likewise assessed in the CD-loop variants of rat α.

The binding constants for each of the variants harboring L85F are denoted by the solid-color bars in Fig. 5. The Ca^{2+} values for the CD and EF sites are presented in panels A and B, respectively. The corresponding Mg^{2+} values are presented in panels C and D. Introduction of L85F into the wild-type protein produces a major increase in $k_{Ca,EF}$, from 1.20×10^8 to $4.82 \times 10^8\ M^{-1}$, a factor of 4.0, while leaving the CD-site value unchanged. Interestingly, the Mg^{2+}-binding constants do not display the same pattern. Although $k_{Mg,EF}$ increases somewhat, from 1.61×10^4 to $2.17 \times 10^4\ M^{-1}$, $k_{Mg,CD}$ falls from 2.05×10^4 to $9.34 \times 10^3\ M^{-1}$.

Fig. 4. Global fit of divalent-ion-binding data for α-PV 49–60. The solid lines represent the optimal fit of the integrated ITC data to an independent two-site model. A comparable level of agreement between the observed and calculated values was observed for all of the proteins described herein. (A) Titration with Ca^{2+} at two protein concentrations: 44 μM (red); 22 μM (green). The occupancies of the EF (green) and CD (red) sites are depicted in the inset as a function of the free Ca^{2+} concentration. (B) Titration of 44 μM samples with Ca^{2+} in the presence of fixed levels of Mg^{2+}: 1.0 mM (cyan); 5.0 mM (magenta); 10.0 mM (blue); 20.0 mM (red). (C) Titration with Ca^{2+}: 44 μM protein plus 60 μM EGTA (red); 56 μM protein plus 60 μM EDTA (green). (D) Titration of 44 μM protein with Ca^{2+} in the presence of 0.1 mM (red) or 1.0 mM (blue) NTA. (E) Titration of 44 μM protein with Mg^{2+} in the absence (cyan) or presence (magenta) of 100 μM EDTA. The occupancies of the EF (green) and CD (red) sites are depicted in the inset as a function of the free Mg^{2+} concentration.

Table 1
Summary of divalent ion-binding properties.

Protein	Ca^{2+} values				Mg^{2+} values			
	$k_{Ca,EF}$[a]	$\Delta H_{Ca,EF}$	$k_{Ca,CD}$[a]	$\Delta H_{Ca,CD}$	$k_{Mg,EF}$[a]	$\Delta H_{Mg,EF}$	$k_{Mg,CD}$[a]	$\Delta H_{Mg,CD}$
	M^{-1}	kcal/mol	M^{-1}	kcal/mol	M^{-1}	kcal/mol	M^{-1}	kcal/mol
Rat α-PV[b]	1.20×10^8	−4.30	1.30×10^8	−1.34	1.61×10^4	0.24	2.05×10^4	7.92
	(1.17, 1.32)	(−4.36, −4.18)	(1.17, 1.32)	(−1.40, −1.28)	(1.56, 2.09)	(0.17,0.30)	(1.56, 2.09)	(7.83, 8.00)
L85F	4.82×10^8	−3.67	1.30×10^8	−3.77	2.17×10^4	4.25	9.34×10^3	4.49
	(3.57, 6.80)	(−3.78, −3.56)	(1.05, 1.57)	(−3.88, −3.65)	(1.91, 2.49)	(4.12, 4.38)	(8.21, 10.6)	(4.36, 4.63)
I49F	1.27×10^8	−4.28	1.10×10^8	−1.76	2.24×10^4	4.01	1.19×10^4	4.62
	(1.13, 1.45)	(−4.36, −4.19)	(0.99, 1.19)	(−1.85, −1.67)	(2.00, 2.54)	(3.89, 4.13)	(1.07, 1.33)	(4.48, 4.76)
I49F-L85F	1.59×10^8	−6.00	1.19×10^8	−2.03	2.13×10^4	2.27	9.41×10^3	5.76
	(1.48, 1.70)	(−6.06, −5.94)	(1.12, 1.27)	(−2.09, −1.97)	(1.89, 2.38)	(2.18, 2.36)	(8.75, 10.1)	(5.64, 5.87)
49–50	2.53×10^8	−8.14	6.23×10^7	−3.05	4.98×10^4	0.01	6.44×10^3	3.47
	(2.30, 2.73)	(−8.23, −8.06)	(5.86, 6.61)	(−3.14, −2.96)	(4.44, 5.59)	(−0.05, 0.07)	(6.05, 7.08)	(3.36, 3.60)
49-50-85	2.70×10^8	−12.2	6.09×10^7	−3.33	3.88×10^4	−3.42	5.90×10^3	2.94
	(2.59, 2.84)	(−12.3, −12.1)	(5.72, 6.57)	(−3.47, −3.23)	(3.60, 4.17)	(−3.52, −3.32)	(5.32, 6.43)	(2.82, 3.08)
49-50-57	2.26×10^8	−8.31	7.10×10^7	−2.81	3.03×10^4	0.04	6.88×10^3	3.29
	(2.13, 2.37)	(−8.39, −8.22)	(6.74, 7.53)	(−2.90, −2.73)	(2.70, 3.36)	(−0.03, 0.11)	(6.40, 7.56)	(3.20, 3.42)
49-50-57-85	1.95×10^8	−12.53	5.68×10^7	−2.84	2.51×10^4	−3.78	5.29×10^3	3.85
	(1.87, 2.05)	(−12.66, −12.41)	(5.45, 5.97)	(−2.93, −2.76)	(2.28, 2.71)	(−3.89, −3.67)	(4.81, 5.92)	(3.74, 4.00)
49–58	1.95×10^8	−5.25	6.14×10^7	−2.61	3.26×10^4	2.27	3.44×10^3	4.96
	(1.83, 2.08)	(−5.30, −5.19)	(5.84, 6.57)	(−2.66, −2.55)	(3.06, 3.55)	(2.23, 2.34)	(3.23, 3.64)	(4.86, 5.06)
49-58/L85F	1.66×10^8	−7.41	4.14×10^7	−2.60	3.21×10^4	0.51	2.10×10^3	5.01
	(1.56, 1.78)	(−7.48, −7.33)	(3.89, 4.39)	(−2.66, −2.53)	(2.91, 3.53)	(0.46, 0.57)	(1.99, 2.23)	(4.91, 5.13)
49–59	1.57×10^8	−4.61	1.09×10^7	−2.00	3.16×10^4	3.16	0.96×10^2	8.66
	(1.43, 1.76)	(−4.70, −4.52)	(1.00, 1.22)	(−2.06, −1.94)	(2.90, 3.44)	(3.07, 3.26)	(0.91, 1.01)	(8.40, 8.83)
49-59/L85F	1.47×10^8	−5.72	1.14×10^7	−1.45	2.78×10^4	2.00	0.90×10^2	8.09
	(1.38, 1.56)	(−5.79, −5.65)	(1.09, 1.21)	(−1.50, −1.38)	(2.60, 2.95)	(1.94, 2.06)	(0.86, 0.97)	(7.88, 8.33)
49–60	1.04×10^8	−6.41	6.03×10^6	−1.52	1.86×10^4	1.40	1.13×10^2	7.52
	(1.00, 1.21)	(−6.59, −6.33)	(5.50, 6.52)	(−1.67, −1.51)	(1.79, 2.25)	(1.15, 1.38)	(1.02, 1.19)	(7.39, 7.92)
49-60/L85F	1.08×10^8	−9.31	7.45×10^6	−1.18	2.09×10^4	−1.46	8.60×10^1	8.07
	(1.00, 1.18)	(−9.42, −9.20)	(6.87, 8.01)	(−1.28, −1.07)	(1.89, 2.33)	(−1.59,-1.34)	(0.77, 0.95)	(7.64, 8.49)
E59D	1.85×10^8	−4.44	1.05×10^7	−1.51	3.64×10^4	3.63	9.87×10^1	9.75
	(1.70, 1.98)	(−4.53, −4.35)	(0.98, 1.14)	(−1.57, −1.45)	(3.42, 3.90)	(3.56, 3.70)	(9.48, 10.3)	(9.55, 9.94)
59–85	1.71×10^8	−5.01	1.25×10^7	−1.52	2.97×10^4	3.63	8.68×10^1	9.55
	(1.59, 1.85)	(−5.11, −4.91)	(1.15, 1.32)	(−1.58, −1.45)	(2.80, 3.18)	(3.52, 3.74)	(8.34, 9.12)	(9.36, 9.83)
59–60	1.62×10^8	−4.85	9.16×10^6	−1.43	3.11×10^4	3.20	1.60×10^2	8.77
	(1.53, 1.74)	(−4.90, −4.80)	(8.61, 9.71)	(−1.47, −1.38)	(2.92, 3.29)	(3.14, 3.26)	(1.54, 1.67)	(8.59, 8.95)
59-60/L85F	1.76×10^8	−5.32	9.83×10^6	−1.70	3.09×10^4	3.07	1.13×10^2	8.86
	(1.63, 1.85)	(−5.37, −5.26)	(9.34, 10.4)	(−1.75,-1.65)	(2.87, 3.24)	(2.98, 3.14)	(1.09, 1.16)	(8.68, 9.03)
Rat β-PV[b]	2.30×10^7	−4.10	1.52×10^6	−3.46	9.23×10^3	3.01	1.68×10^2	4.16
	(2.05, 2.56)	(−4.16, −4.06)	(1.38, 1.70)	(−3.52, −3.41)	(8.93, 9.66)	(2.97, 3.05)	(1.58, 1.79)	(4.00, 4.32)
β D59E	3.15×10^7	−6.02	2.01×10^6	−1.29	1.65×10^4	1.53	1.86×10^2	5.18
	(2.90, 3.41)	(−6.14, −5.90)	(1.85, 2.19)	(−1.36, −1.21)	(1.51, 1.82)	(1.42, 1.64)	(1.67, 2.09)	(4.98, 5.39)
β 59–85	4.90×10^7	−6.28	4.04×10^6	−1.34	3.17×10^4	0.92	2.13×10^2	6.69
	(4.60, 5.29)	(−6.34, −6.21)	(3.80, 4.33)	(−1.41, −1.29)	(2.98, 3.39)	(0.86, 0.99)	(2.02, 2.25)	(6.55, 6.82)

[a] Microscopic binding constants at 25 °C in Hepes-buffered saline, pH 7.4, with 90% confidence intervals shown in parentheses.
[b] Data from Henzl et al. (2004), *Biochemistry 43*, 2747–2763.

Otherwise, the changes in divalent-ion-binding affinity provoked by the L85F mutation are modest, with no obvious pattern. For example, in the I49F variant, whereas both Ca^{2+}-binding constants increase, both Mg^{2+}-binding constants decrease. By contrast, in α 49–57, all four binding constants decrease. And in the α 49–59 background, whereas $k_{Ca,EF}$ and $k_{Mg,EF}$ both decrease, $k_{Ca,CD}$ increases slightly, and $k_{Mg,CD}$ decreases slightly. The largest perturbations attendant to the L85F substitution, −33% and −39%, are associated with $k_{Ca,CD}$ and $k_{Mg,CD}$, respectively, in the α 49–58 variant. For the most part, the changes are considerably smaller.

2.3. Binding enthalpies: CD-loop variants

The ΔH_{Ca} values are plotted in Fig. 6A for each of the α-PV variants included in this study. Data for the CD-loop variants are represented by the cross-hatched columns – red for the EF site, green for the CD site, and blue for the overall enthalpy change. The numerical values are listed in Table 2. Although the changes in binding enthalpy that accompany the CD-loop mutations are generally small, two of the substitutions produce major changes in binding enthalpy. Upon introduction of L50I into α I49F, the overall binding enthalpy drops from −6.04 to −11.19 kcal mol^{-1}. Then, subsequent introduction of I58L into α 49–57 returns the total enthalpy change to −7.86 kcal mol^{-1}. In each of these cases, the bulk of the change is associated with the EF-site-binding event. Introduction of E59D into α 49–58 causes a further decrease in the magnitude of ΔH, to −6.61 kcal mol^{-1}. Finally, introduction of E60G into α 49–59 returns the toal ΔH_{Ca} value to −7.93 kcal mol^{-1}. In the absence of the other CD-loop mutations, the $\Delta\Delta H$ values resulting from E59D and E60G are substantially smaller.

The changes in ΔH_{Mg} (Fig. 6B) largely mirror those observed for ΔH_{Ca}, with major changes associated with L50I and I58L. However, whether introduced into wild-type α or the α 49–58 variant, E59D has a substantially greater impact on ΔH_{Mg} than on ΔH_{Ca}. Similarly, whereas I49F leaves the Ca^{2+}-binding enthalpies nearly unchanged, the mutation seriously perturbs the Mg^{2+}-binding enthalpies associated with both sites.

2.4. Binding enthalpies: L85F variants

The Ca^{2+}-binding enthalpies for α L85F and the α CD-loop variants harboring the L85F mutation are represented by the solid-color columns in Fig. 6A – with ΔH_{EF}, ΔH_{CD}, and ΔH_{total} rendered in red, green, and blue, respectively. Corresponding data for Mg^{2+} are plotted in Fig. 6B.

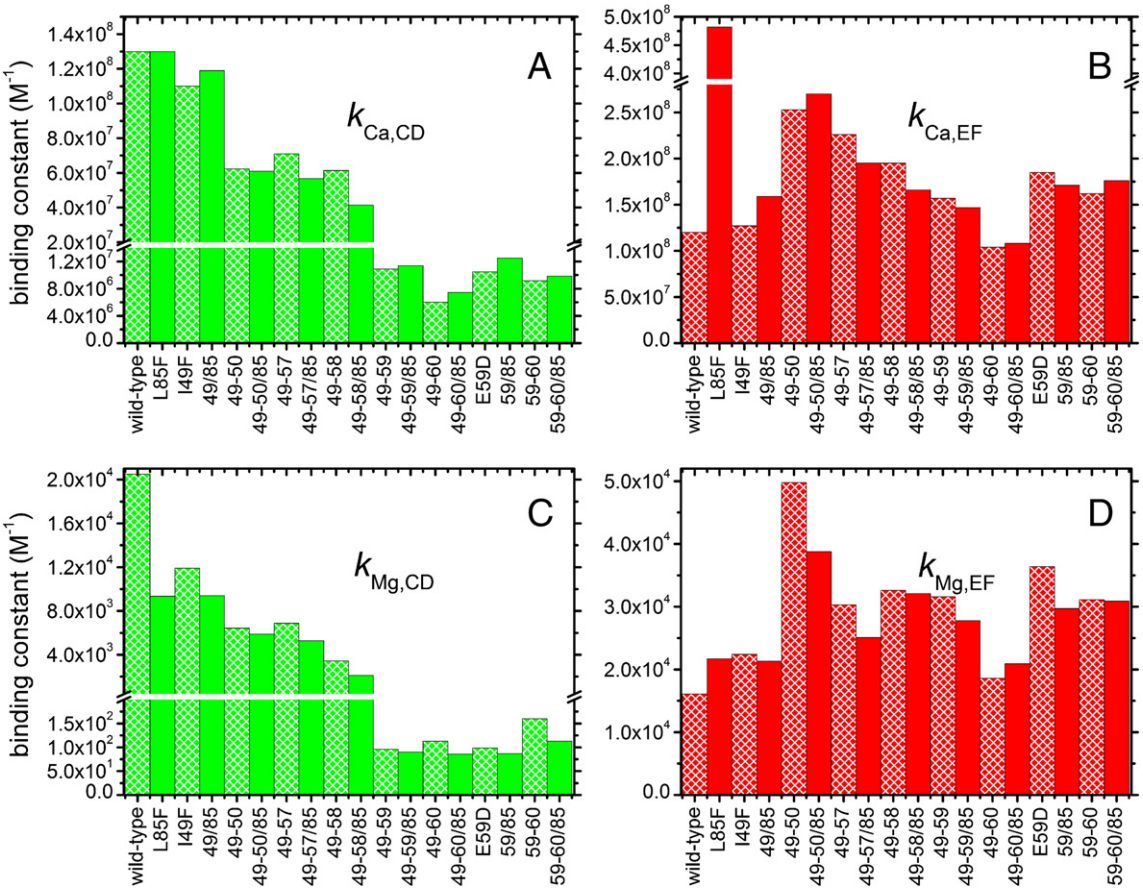

Fig. 5. Binding constants in the α CD-loop and α L85F variants. The data for the CD- and EF sites are displayed in green and red, respectively, a convention maintained throughout the paper. In addition to the color coding, cross-hatching is used to distinguish data for the proteins lacking the L85F mutation. (A) Ca^{2+}-binding constants for the α-PV CD site. (B) Ca^{2+}-binding constants for the EF site. (C) Mg^{2+}-binding constants for the CD site. (D) Mg^{2+}-binding constants for the EF site. Vertical breaks have been inserted in panels A and C, to more effectively display the diminished binding constants observed in the variants harboring the E59D mutation. A vertical break has also been included in panel B, to place the height of the bar for the L85F variant on a similar scale to those for the other variants.

Although the L85F mutation has relatively little effect on divalent-ion-binding affinity in the α CD-loop variants, the substitution strongly perturbs both Ca^{2+}- and Mg^{2+}-binding enthalpies in the majority of the variants.

Major increases in exothermicity are observed for the α 49–50/85 and α 49–57/85 variants, which exhibit total Ca^{2+}-binding enthalpies of −15.5 and −15.4 kcal mol^{-1}, respectively. The L85F mutation also produces substantial increases in exothermicity in the α I49F, α 49–58, and α 49–60 backgrounds. Total Ca^{2+}-binding enthalpies for α 49/85, α 49–58/85, and α 49–60/85 are −8.0, −10.0, and −10.5 kcal mol^{-1}, respectively. In each of these, the enthalpy change associated with the EF-site-binding event is the more strongly perturbed. Interestingly, L85F has a much smaller impact on Ca^{2+}-binding enthalpy in the α 49–59, α E59D, and α 59–60 backgrounds.

The pattern of changes in Mg^{2+}-binding enthalpy roughly parallels that seen with Ca^{2+}. As observed for Ca^{2+}, the L85F mutation more strongly impacts the EF-site. Because the total Mg^{2+}-binding enthalpies are positive, the effect of L85F is to decrease their magnitude – i.e., render them less endothermic. In fact, the EF-site binding events are actually exothermic in α 49–50/85, α 49–57/85, and α 49–60/85.

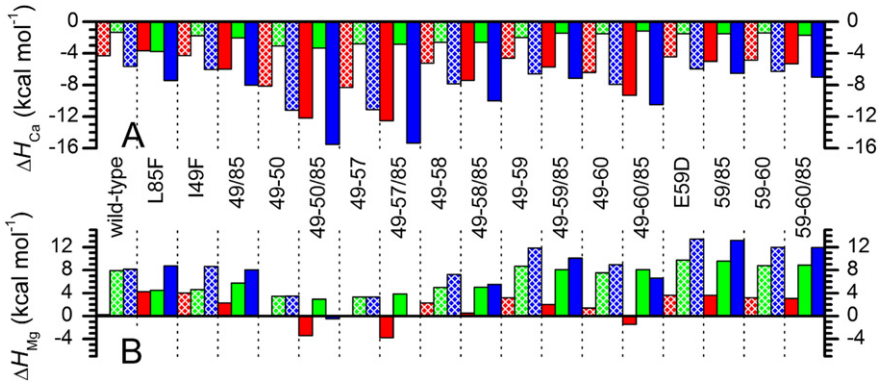

Fig. 6. Binding-enthalpies for Ca^{2+} (A) and Mg^{2+} (B). Data for the EF-site are shown in red; data for the CD-site are shown in green; and the total binding enthalpy is displayed in blue. Cross-hatched columns denote data for the CD-loop mutations; solid colors denote data for the CD-loop variants plus L85F.

Table 2
Divalent ion-binding energetics.[a]

	Ca^{2+} binding			Mg^{2+} binding		
Protein	ΔG	ΔH	−TΔS	ΔG	ΔH	-TΔS
EF Site						
αPV	−11.02	−4.30	−6.72	−5.74	0.24	−5.98
αPV L85F	−11.84	−3.67	−8.17	−5.91	4.25	−10.16
αPV I49F	−11.05	−4.28	−6.77	−5.93	4.01	−9.94
αPV 49/85	−11.18	−6.00	−5.18	−5.90	2.27	−8.17
αPV 49–50	−11.46	−8.14	−3.32	−6.40	0.010	−6.41
αPV 49–50/85	−11.50	−12.20	0.70	−6.26	−3.42	−2.84
αPV 49–57	−11.39	−8.31	−3.08	−6.11	0.040	−6.15
αPV 49–57/85	−11.30	−12.53	1.23	−6.00	−3.78	−2.22
αPV 49–58	−11.30	−5.25	−6.05	−6.15	2.27	−8.42
αPV 49–58/85	−11.21	−7.41	−3.80	−6.14	0.51	−6.65
αPV 49–59	−11.17	−4.61	−6.56	−6.13	3.16	−9.29
αPV 49–59/85	−11.14	−5.72	−5.42	−6.06	2.00	−8.06
αPV 49–60	−10.93	−6.41	−4.52	−5.82	1.40	−7.22
αPV 49–60/85	−10.95	−9.31	−1.64	−5.89	−1.46	−4.43
αPV E59D	−11.27	−4.44	−6.83	−6.22	3.63	−9.85
αPV 59/85	−11.23	−5.01	−6.22	−6.10	3.63	−9.73
αPV 59–60	−11.19	−4.85	−6.34	−6.13	3.20	−9.33
αPV 59–60/85	−11.24	−5.32	−5.92	−6.12	3.07	−9.19
βPV	−10.04	−4.10	−5.94	−5.41	3.01	−8.42
βPV D59E	−10.22	−6.02	−4.20	−5.75	1.53	−7.28
βPV 59/85	−10.49	−6.28	−4.21	−6.14	0.92	−7.06
CD Site						
αPV	−11.06	−1.34	−9.72	−5.88	7.92	−13.80
αPV L85F	−11.06	−3.77	−7.29	−5.41	4.49	−9.90
αPV I49F	−10.96	−1.76	−9.20	−5.56	4.62	−10.18
αPV 49/85	−11.01	−2.03	−8.98	−5.42	5.76	−11.18
αPV 49–50	−10.63	−3.05	−7.58	−5.19	3.47	−8.66
αPV 49–50/85	−10.61	−3.33	−7.28	−5.14	2.94	−8.08
αPV 49–57	−10.70	−2.81	−7.89	−5.23	3.29	−8.52
αPV 49–57/85	−10.57	−2.84	−7.73	−5.08	3.85	−8.93
αPV 49–58	−10.62	−2.61	−8.01	−4.82	4.96	−9.78
αPV 49–58/85	−10.39	−2.60	−7.79	−4.53	5.01	−9.54
αPV 49–59	−9.59	−2.00	−7.59	−2.70	8.66	−11.36
αPV 49–59/85	−9.62	−1.45	−8.17	−2.66	8.09	−10.75
αPV 49–60	−9.24	−1.52	−7.72	−2.80	7.52	−10.32
αPV 49–60/85	−9.37	−1.18	−8.19	−2.64	8.07	−10.71
αPV E59D	−9.57	−1.51	−8.06	−2.72	9.75	−12.47
αPV 59/85	−9.68	−1.52	−8.16	−2.64	9.55	−12.19
αPV 59–60	−9.49	−1.43	−8.06	−3.00	8.77	−11.77
αPV 59–60/85	−9.53	−1.70	−7.83	−2.80	8.86	−11.66
βPV	−8.43	−3.46	−4.97	−3.03	4.16	−7.19
βPV D59E	−8.59	−1.29	−7.30	−3.09	5.18	−8.27
βPV 59/85	−9.01	−1.34	−7.67	−3.17	6.69	−9.86
Total						
αPV	−22.08	−5.64	−16.44	−11.61	8.16	−19.77
αPV L85F	−22.90	−7.44	−15.46	−11.33	8.74	−20.07
αPV I49F	−22.01	−6.04	−15.97	−11.49	8.63	−20.12
αPV 49/85	−22.19	−8.03	−14.16	−11.32	8.03	−19.35
αPV 49–50	−22.08	−11.19	−10.89	−11.60	3.48	−15.08
αPV 49–50/85	−22.11	−15.53	−6.58	−11.40	−0.48	−10.92
αPV 49–57	−22.09	−11.12	−10.97	−11.34	3.33	−14.67
αPV 49–57/85	−21.88	−15.37	−6.51	−11.08	0.07	−11.15
αPV 49–58	−21.92	−7.86	−14.06	−10.98	7.23	−18.21
αPV 49–58/85	−21.59	−10.01	−11.58	−10.67	5.52	−16.19
αPV 49–59	−20.77	−6.61	−14.16	−8.84	11.82	−20.66
αPV 49–59/85	−20.76	−7.17	−13.59	−8.72	10.09	−18.81
αPV 49–60	−20.18	−7.93	−12.25	−8.62	8.92	−17.54
αPV 49–60/85	−20.32	−10.49	−9.83	−8.53	6.61	−15.14
αPV E59D	−20.84	−5.95	−14.89	−8.94	13.38	−22.32
αPV 59/85	−20.90	−6.53	−14.37	−8.74	13.18	−21.92
αPV 59–60	−20.68	−6.28	−14.40	−9.13	11.97	−21.10
αPV 59–60/85	−20.78	−7.02	−13.76	−8.92	11.93	−20.85
βPV	−18.47	−7.56	−10.91	−8.44	7.17	−15.61
βPV D59E	−18.82	−7.31	−11.51	−8.85	6.71	−15.56
βPV 59/85	−19.49	−7.62	−11.87	−9.31	7.61	−16.92

[a] All energies in kcal mol^{-1}.

The largest changes in $\Delta H_{Mg,total}$ produced by L85F are observed in the α 49–50/85 and α 49–57/85 variants, but significant changes are also observed when L85F is introduced into either α 49–58, α 49–59, or α 49–60. The enthalpic perturbation is much smaller in the α E59D and α 59–60 variants, in which the canonical residues reside at positions 49, 50, 57, and 58. Although the change in $\Delta H_{Mg,total}$ is likewise small when L85F is introduced into α I49F, it is the result of substantial, but nearly offsetting, changes in the Mg^{2+} enthalpies for the EF- and CD sites.

Interestingly, when L85 is replaced by phenylalanine in wild-type α, it is the Ca^{2+}-binding event associated with the CD-site, rather than the EF-site, that is rendered more exothermic. The EF-site enthalpy actually decreases slightly in magnitude. The mutation also strongly perturbs both Mg^{2+}-binding enthalpies in the wild-type background. The CD-site enthalpy in α L85F is decidedly less endothermic, the EF-site enthalpy decidedly more endothermic.

2.5. Estimates of ΔC_P for Ca^{2+} binding by select variant proteins

As noted above, a subset of the mutations examined in this study cause Ca^{2+}-binding to become substantially more exothermic. To gain insight into the origin of these large $\Delta\Delta H$ values, several of the proteins were also titrated with Ca^{2+} at 5 °C, to obtain an estimate of the changes in heat-capacity that accompany metal ion-binding. Table 3 presents the total Ca^{2+}-binding enthalpies at 5 and 25 °C, the estimated heat-capacity changes, and the differences between the observed ΔC_p value and that of the wild-type α-PV – i.e., $\Delta\Delta C_p$.

The very small change in heat-capacity (−0.01 kcal mol^{-1} K^{-1}) that accompanies Ca^{2+} binding to wild-type rat α-PV [12] balloons to −0.20 kcal mol^{-1} K^{-1} with the introduction of I49F and L50I. Further mutation of residues Y57 and I58, to produce α 49–58, substantially reduces the magnitude of the heat-capacity change (to −0.082 kcal mol^{-1} K^{-1}), and subsequent introduction of E59D further diminishes ΔC_p and reverses its sign.

Replacement of L85 by phenylalanine in the α 49–50 background causes an additional increase in the magnitude of the heat-capacity change associated with Ca^{2+} binding. Whereas α 49–50 displays a ΔC_p of −0.20 kcal mol^{-1} K^{-1}, the α 49–50/85 variant displays a ΔC_p of −0.34. By contrast, L85F has no discernible effect on ΔC_p when introduced into the α 49–59 background.

2.6. Differential scanning calorimetry on select α-PV variants

The relative stabilities of several of the Ca^{2+}-free proteins were assessed by DSC in phosphate-buffered saline (PBS) containing 1.0 mM EDTA. Fig. 7 displays the resulting excess-heat-capacity curves (–), produced by first subtracting the buffer scan from the raw protein-denaturation data, then subtracting the transition baseline. Estimates for the melting temperature (T_m) and van't Hoff denaturational enthalpy (ΔH_{vH}) were obtained by fitting the excess-heat-capacity curves to a two-state unfolding model, as described in Materials and Methods. Integration of the excess-heat-capacity curve yielded an estimate for the calorimetric denaturational enthalpy (ΔH_{cal}). Table 4 lists the T_m, ΔH_{vH}, and ΔH_{cal} values.

Wild-type rat recombinant α-PV denatures at 45.2 °C in PBS-EDTA buffer [24]. The combined I49F and L50I mutations substantially lower

Table 3
Temperature-dependence of total Ca^{2+}-binding enthalpies.

	Total enthalpy (kcal mol^{-1})		ΔC_p (kcal mol^{-1} K^{-1})	$\Delta\Delta C_p$ (kcal mol^{-1} K^{-1})
Protein	5 °C	25 °C		
Rat α-PV	−5.46	−5.64	−0.01	--
α 49-50	−7.24	−11.19	−0.20	−0.19
α 49-58	−6.22	−7.86	−0.082	−0.07
α 49-59	−7.00	−6.62	0.019	0.03
α 49-50/85	−8.76	−15.53	−0.34	−0.33
α 49-59/85	−7.54	−7.17	0.018	0.03

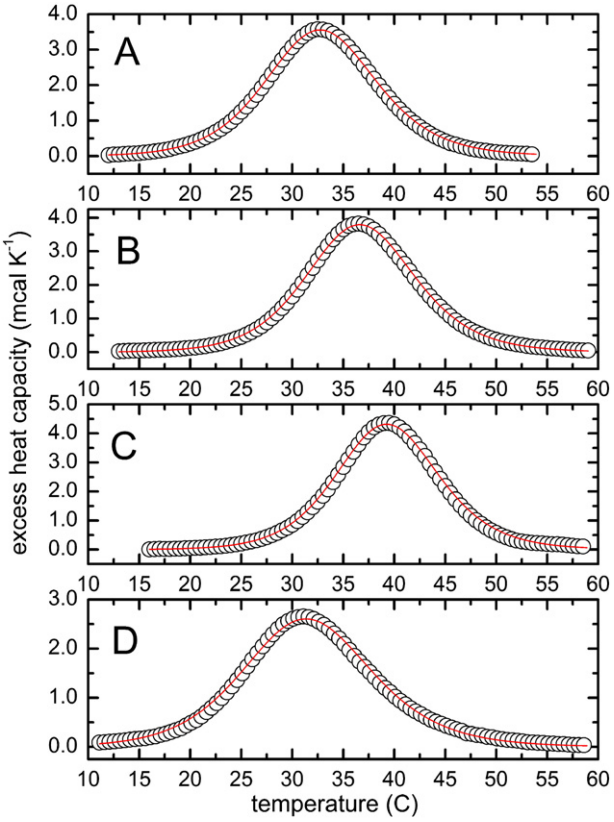

Fig. 7. DSC analysis of several rat α-PV variants. (A) α 49–50. (B) α 49–58. (C) α 49–59. (D) α 49-50/85.

the T_m, to 32.9 °C, and the addition of L85F to the α 49–50 background decreases the melting temperature still further, to 31.6 °C. However, introduction of the other CD-loop mutations – to produce α 49–58 and, then, α 49–59 – appear to restore stability to the molecule – increasing the T_m to 36.8 and 39.4 °C, respectively.

3. Discussion

A previous study on rat β-PV revealed that the non-consensus CD-loop residues in that protein – i.e., at positions 49, 50, 57, 58, 59, and 60 – influence divalent-ion affinity. However, their impact is strongly modulated by the identity of residue 85. This work was undertaken to assess the generality of the earlier findings and has yielded several interesting observations. For convenience, a shorthand notation is introduced to denote the residues present at the six CD-loop positions and at position 85. For example, IL…FIEE/L and FI…YLDG/L indicate the configurations in the wild-type α- and β isoforms, respectively.

The changes in Gibbs energy resulting from the CD-loop mutations, relative to the wild-type proteins, are displayed in Fig. 8. The red, green, and blue columns represent the EF-site, CD-site, and overall $\Delta\Delta G$ values, respectively. Data for rat α are presented in panels A (Ca^{2+}) and C (Mg^{2+}); data for rat β are presented in panels B (Ca^{2+}) and D (Mg^{2+}). Table 2 lists the ΔG, ΔH, and $-T\Delta S$ values that accompany binding of Ca^{2+} and Mg^{2+} to each of the proteins examined in this work. Several points merit emphasis.

Table 4
Thermal stability parameters of select α-PV variants.

protein	T_m (Celsius)	ΔH_{vH} (kcal mol^{-1})	ΔH_{cal} (kcal mol^{-1})
α 49–50	32.9 ± 0.4	51.0 ± 2.5	50.5 ± 2.7
α 49–50/85	31.6 ± 0.4	43.8 ± 2.2	44.7 ± 2.4
α 49–58	36.8 ± 0.4	53.8 ± 2.6	54.6 ± 3.1
α 49–59	39.4 ± 0.4	57.9 ± 2.8	56.3 ± 2.5

3.1. The impact of the combined CD-loop mutations is restricted to the CD site

A priori, we anticipated that the CD-loop mutations would reduce the affinity of the rat α isoform for Ca^{2+} and Mg^{2+}. However, although the CD-site behavior is in accordance with expectation, EF-site divalent-ion affinity improves in nearly every case. The sole exception is the α 49–60, which displays a minor reduction in Ca^{2+} affinity. These results contrast strikingly with the corresponding mutations in the rat β platform, where the CD-loop mutations produce significant improvements in affinity at both binding sites.

3.2. Mg^{2+} affinity is more strongly attenuated than Ca^{2+} affinity by the CD-loop mutations

The reductions in CD-site Mg^{2+} affinity resulting from the CD-loop mutations in rat α largely parallel the reductions in CD-site Ca^{2+} affinity. However, they are larger in magnitude. Thus, the Ca^{2+} affinity in α 49–60 ($K_{Ca,CD} = 6.0 \times 10^6$ M^{-1}) remains substantially higher than that of the β-PV isoform (1.5×10^6 M^{-1}), whereas the Mg^{2+} affinity ($K_{Mg,CD} = 113$ M^{-1}) is reduced to a level comparable to, in fact lower than, that observed in wild-type β (168 M^{-1}).

EF-hand motifs are commonly classified as Ca^{2+}/Mg^{2+} sites ($K_{Ca} \geq 10^7$ M^{-1}; $K_{Ca} \geq 10^4$ M^{-1}) or Ca^{2+}-specific sites ($K_{Ca} < 10^7$ M^{-1}; $K_{Mg} < 10^3$ M^{-1}). The former – also called "high-affinity" or "mixed" sites – occur in proteins that function primarily as Ca^{2+} buffers. The structural perturbations that accompany occupation of Ca^{2+}/Mg^{2+} sites are generally minor. Ca^{2+}-specific sites, on the other hand, are typically present in Ca^{2+}-sensors. In those proteins, occupation of the Ca^{2+}-specific site triggers a conformational change that promotes interaction with effector proteins. The combined CD-loop mutations transform the CD site in rat α-PV from a Ca^{2+}/Mg^{2+} site to Ca^{2+}-specific one. In fact, as discussed below, the E59D mutation alone is sufficient to produce the Ca^{2+}-specific divalent-ion-binding signature.

3.3. D-E exchange at residue 59

With just one exception, the *–x* ligand in the parvalbumin CD site is a glutamyl carboxylate. The mammalian β isoform is the sole exception, replacing glutamate with aspartate. Because the shorter aspartyl side-chain is unable to directly coordinate the bound ion, a water molecule serves as the proximal ligand. Initially, there was speculation that this single difference was responsible for the attenuated divalent-ion affinity of rat β-PV. In fact, it is not that simple. Restoration of glutamate at the *–x* position in the CD site, via the D59E mutation, yields only a nominal increase in divalent ion affinity in wild-type β [18,25]. Paradoxically, however, the E59D mutation produces major decreases in the Ca^{2+}- and Mg^{2+} affinities of rat of α-PV, and the impact of the mutation is largely independent of the CD-loop mutations at residues 49, 50, 57, and 58.

Inspection of the data suggests that the impact of D59-E59 exchange is maximized by juxtaposing the canonical CD-loop residues with F85. Thus, replacement of D59 by glutamate in the context of β49–58/85 (IL…FIDG/F) raises Ca^{2+} affinity by 0.73 kcal mol^{-1}, as compared to 0.35 kcal mol^{-1} in wild-type β (IL…FIDG/L). This result suggests that D59E might produce still greater improvement in the rat β variant harboring the IL…FIDE/F configuration. Likewise, the overall $\Delta\Delta G$ of 2.00 kcal mol^{-1} that accompanies the E59D mutation in α L85F (IL…FIEE/F) substantially exceeds the 1.24 kcal mol^{-1} measured in the wild-type background (IL…FIEE/L). Given that phenylalanine is the consensus residue at position 85 in the β sub-lineage, one would predict

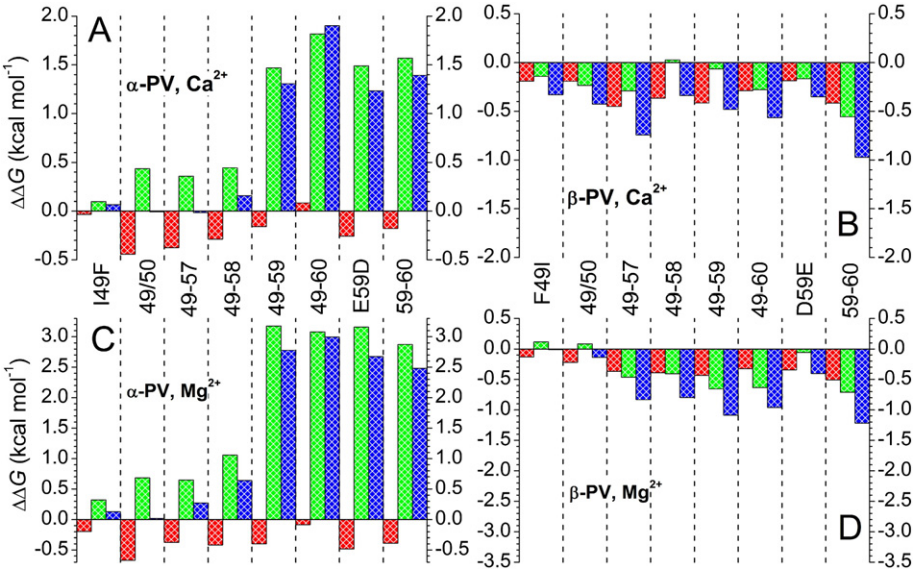

Fig. 8. Changes in Gibbs energy of binding, relative to the wild-type proteins, for the site-specific variants of rat α-PV (panels A, C) and rat β-PV (panels B, D). Data for the EF- and CD-sites are displayed in red and green, respectively. The total change in Gibbs energy is depicted in blue. Cross-hatching is included to emphasize that these proteins lack the L85F mutation. (A) $\Delta\Delta G$ values for binding of Ca^{2+} to rat α-PV. (B) $\Delta\Delta G$ values for binding of Ca^{2+} to rat β-PV. (C) $\Delta\Delta G$ values for binding of Mg^{2+} to rat α-PV. (D) $\Delta\Delta G$ values for binding of Mg^{2+} to rat β-PV.

that E59D should produce a major attenuation of divalent-ion-affinity in a β-PV isoform harboring the canonical CD-loop configuration.

3.4. E-G exchange at residue 60

Unlike the other five non-consensus CD-loop residues in rat β-PV, G60 is not strongly conserved in other mammalian β isoforms. For example, in the mouse and human proteins, glutamate appears at position 60. However, because the identity of residue 60 significantly influences divalent-ion-affinity in the rat β-PV, it was included in this study.

As in the rat β isoform, the identity of residue 60 likewise influences divalent-ion affinity in rat α. The impact of the E-G exchange is somewhat context-dependent. Whereas introduction of the E60G mutation into the α 49–59 background (FI…YLDE/L) lowers Ca^{2+} affinity by 0.59 kcal mol^{-1}, if the mutation is performed in the context of E59D alone (IL…FIDE/L), Ca^{2+} affinity is lowered by just 0.06 kcal mol^{-1}. The G60E mutation in the β isoform exhibits a similar response to context. When performed in β 49–59 (IL…FIEG/L), the mutation raises Ca^{2+} affinity by just 0.08 kcal mol^{-1}. However, when it is performed in the presence of D59E alone (FI…YLEG), Ca^{2+} affinity improves by 0.62 kcal mol^{-1}. Thus, in both protein platforms, D-E exchange at residue 60 has a greater impact when positions 49, 50, 57, and 58 are occupied by the non-consensus residues – Phe, Ile, Tyr, and Leu.

3.5. Response to the L85F mutations

The alterations in Gibbs energy binding resulting from introduction of the L85F mutation into each of the α-PV CD-site variants are displayed in Fig. 9A and C for Ca^{2+} and Mg^{2+}, respectively. Corresponding data for the rat β isoform are presented in panels B and D. As before, the resulting changes in Gibbs energy – EF-site, CD-site, and total – are represented by red, green, and blue bars, respectively. The data have been scaled identically to facilitate comparison.

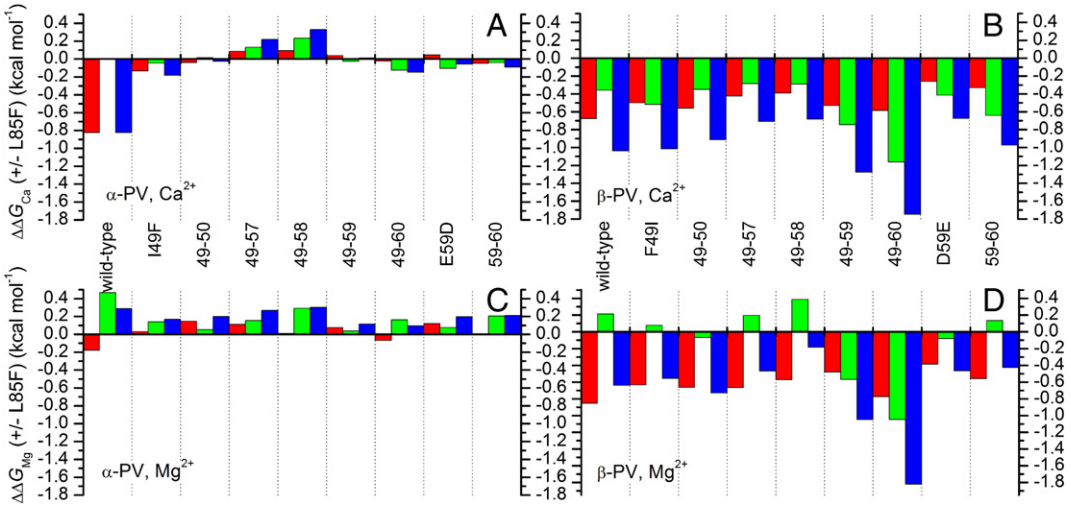

Fig. 9. Impact of the L85F mutation in rat α-PV (panels A, C) and rat β-PV (panels B, D). The $\Delta\Delta G$ values represent the difference in the Gibbs energies for binding of Ca^{2+} or Mg^{2+} resulting from introduction of the L85F mutation – i.e., $\Delta G_{x/85} - \Delta G_x$, where *x* denotes the protein of interest. (A) $\Delta\Delta G_{Ca}$ for rat α-PV. (B) $\Delta\Delta G_{Ca}$ for rat β-PV. (C) $\Delta\Delta G_{Mg}$ for rat α-PV. (D) $\Delta\Delta G_{Mg}$ for rat β-PV. The red- and green columns represent the changes in Gibbs energy for the EF- and CD sites, respectively; the blue columns represent the total change in Gibbs energy. The panels have been scaled identically for ease of comparison.

In the rat β-PV background, the L85F mutation uniformly increases Ca^{2+} affinity, with significant improvements observed at both sites. In wild-type β (FI…YLDG/L), overall Ca^{2+} affinity increases by 1.04 kcal mol^{-1}. Although the improvement dips to 0.68 kcal mol^{-1} in β 49–58 (IL…FIDG/L), it rises to 1.75 kcal mol^{-1} when the other five CD-loop substitutions are present (IL…FIEE/L). In the absence of D59E, replacement of L85 by phenylalanine generally has a larger effect on EF-site Ca^{2+} affinity. However, in the presence of E59, CD-site affinity exhibits the greater increase. Overall Mg^{2+} affinity largely parallels Ca^{2+} affinity. However, CD-site Mg^{2+} affinity is reduced (or nearly unchanged) unless all six CD-loop mutations are present.

Replacement of L85 with phenylalanine has a major impact in wild-type rat α-PV (IL…FIEE/L), improving EF-site Ca^{2+} affinity by 0.82 kcal mol^{-1}. However, the influence of L85F on the CD-loop variants ranges from small to negligible. Simply replacing I49 by Phe (FL…FIEE/L) seriously dampens the effect of L85F, and the introduction of I50L (FI…FIEE/L) essentially abolishes its impact. These observations imply an interaction between the side-chains of residues 49, 50, and 85. With incorporation of additional mutations at positions 57 and 58, the L85F mutation once more produces a minor reduction in Ca^{2+} affinity, but the changes are dwarfed by those observed in β. Interestingly, the single E59D mutation (IL…FIDE/L) similarly erases the effect of L85F on the EF site – additional evidence of communication between the CD loop and residue 85. With respect to Mg^{2+} affinity, L85F also has its largest effect on the wild-type protein. However, in contrast with Ca^{2+}, overall Mg^{2+} affinity declines (by 0.28 kcal mol^{-1}), in this case primarily due to a reduction in Mg^{2+} affinity at the CD site. In the α CD-loop variants, L85F yields small (≤0.3 kcal mol^{-1}) decreases in Mg^{2+} affinity.

In summary, L85F exerts its maximal effect in wild-type α, substantially increasing the EF-site Ca^{2+} affinity. However, any departure from the canonical CD-loop configuration (IL…FIEE) reduces its impact on binding free energy. In the β platform, the increase in divalent ion affinity that accompanies replacement of L85 by phenylalanine is greater in the β 49–60 variant (IL…FIEE) than in 59–60 (FI…YLEE). Similarly, L85F produces a much greater impact in β 49–59 (IL…FIEG) than in β D59E (FI…YLEG). Evidently, the consequences of L-F substitution at residue 85 are maximized when the constellation of CD-loop residues resembles that in the wild-type α isoform.

3.6. Enthalpy changes

The alterations in Δ*H* resulting from the CD-loop and L85F mutations have been plotted in Fig. 10 for both isoforms – α in panels A-D, β in panels E-H. As in previous figures, data for the EF- and CD sites are colored red and green, respectively, and the total ΔΔ*H* is rendered in blue. Sizable ΔΔ*H* values are observed for both proteins. However, there are two noteworthy differences. Whereas substantial ΔΔ*H* effects in the β system are accompanied by substantial changes in binding affinity, the mutations that produce the largest ΔΔ*H* values in the α background have little effect on divalent-ion affinity. Additionally, with just one exception, mutations in the β isoform perturb the enthalpies associated with both binding sites. By contrast, in the α isoform, the changes in Δ*H* are largely restricted to the EF site. In the following paragraphs, we analyze the source of the large ΔΔ*H* values for several α-PV variants.

3.7. The α 49–50 variant

Although the combined I49F and L50I mutations have a negligible impact of the overall Gibbs energy of Ca^{2+} binding ($\Delta\Delta G_{total} \approx 0$), the total Ca^{2+}-binding enthalpy drops by 5.55 kcal mol^{-1}, to −11.19 kcal mol^{-1} (Table 2). Significantly, binding is less exothermic at 5 °C, just −7.24 kcal mol^{-1} (Table 3), which translates to a ΔC_p of −0.20 kcal K^{-1} mol^{-1}. In wild-type α, the corresponding heat-capacity change is much smaller (−0.01 kcal K^{-1} mol^{-1}) [12]. Thus, the I49F and L50I mutations produce a $\Delta\Delta C_p$ value of −0.19 kcal K^{-1} mol^{-1}.

The total entropy change due to Ca^{2+} binding can be expressed as

$$\Delta S_{bind} = \Delta S_{solv} + \Delta S_{rt} + \Delta S_{conf} \quad (7)$$

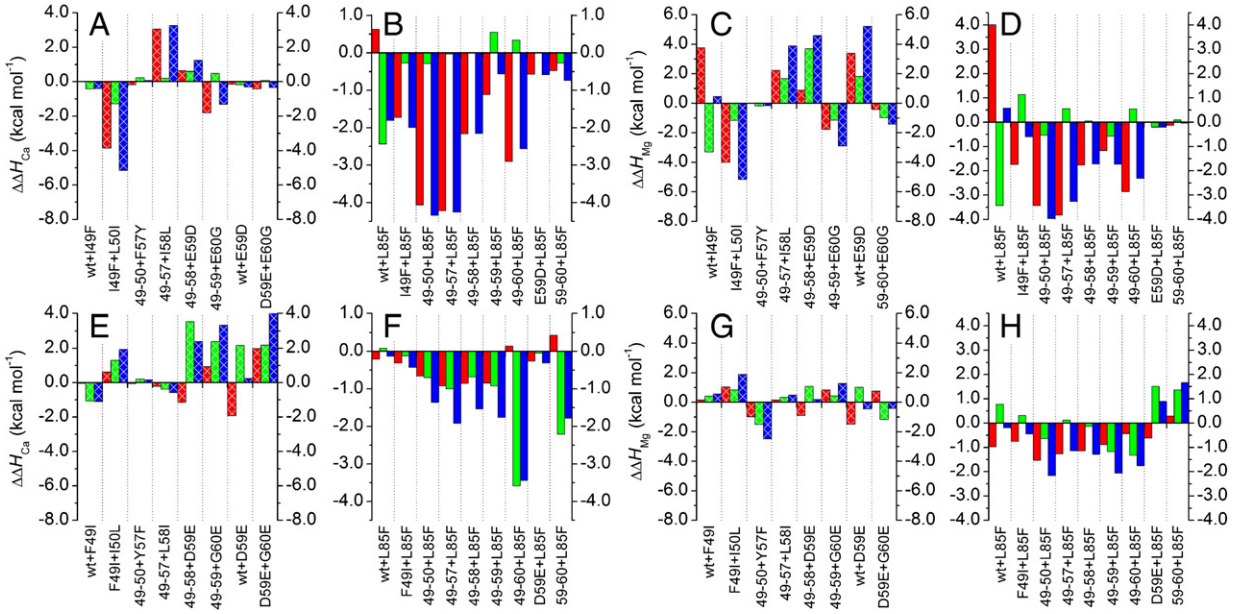

Fig. 10. Perturbation of binding-enthalpies resulting from the mutations in rat α-PV (panels A-D) and in rat β-PV (panels E-H). (A) $\Delta\Delta H_{Ca}$ values resulting from the CD-loop mutations in rat α. (B) $\Delta\Delta H_{Ca}$ values produced by L85F in wild-type α and the CD-loop variants. (C) $\Delta\Delta H_{Mg}$ values resulting from the CD-loop mutations in α. (D) $\Delta\Delta H_{Mg}$ values produced by L85F in wild-type α and the CD-loop variants. (E) $\Delta\Delta H_{Ca}$ values resulting from the CD-loop mutations in rat β. (F) $\Delta\Delta H_{Ca}$ values produced by L85F in wild-type β and the CD-loop variants. (G) $\Delta\Delta H_{Mg}$ values resulting from the CD-loop mutations in rat β. (H) $\Delta\Delta H_{Mg}$ values produced by L85F in wild-type β and the CD-loop variants. The red- and green columns reflect the data for the EF- and CD sites, respectively; the blue columns represent the total ΔΔ*H* values.

where ΔS_{solv} represents the contribution due to changes in solvation, ΔS_{rt} the contribution due to altered rotational/translational motion, and ΔS_{conf} the contribution due to ligation-associated conformational change. Because wild-type α and α 49–50 should have identical rotational-translational components, if one subtracts the ΔS_{bind} values for the two proteins, the remainder should reflect the differences in the solvation and conformational components:

$$\Delta\Delta S_{bind} = \Delta\Delta S_{solv} + \Delta\Delta S_{conf} \tag{8}$$

Rearrangement of Eq. (8) yields an expression for $\Delta\Delta S_{conf}$:

$$\Delta\Delta S_{conf} = \Delta\Delta S_{bind} - \Delta\Delta S_{solv} \tag{9}$$

The entropy of solvation approaches zero at 385 K, permitting an estimate for the solvation entropy at 25 °C by the following relationship [26,27]

$$\Delta S_{solv} = \Delta C_p \ln\left(\frac{298.15}{385.15}\right) \tag{10}$$

By extension, the difference in solvation entropy between α 49–50 and wild-type α-PV should be approximately equal to

$$\Delta\Delta S_{solv} = \Delta\Delta C_p \ln\left(\frac{298.15}{385.15}\right) \tag{11}$$

Substituting the $\Delta\Delta C_p$ value of -0.19 kcal K^{-1} mol^{-1} derived above yields an estimate for $\Delta\Delta S_{solv}$ of 49 cal K^{-1} mol^{-1}.

The difference in overall binding entropy at 25 °C, $\Delta\Delta S_{bind}$, is -19 cal K^{-1} mol^{-1} for the two proteins (Table 2). Thus, according to Eq. (9), $\Delta\Delta S_{conf}$ equals -68 cal K^{-1} mol^{-1}. It has been suggested [28] that the number of residues associated with a ligation-linked folding transition is approximately

$$N_{fold} = \frac{\Delta S_{conf}}{-5.6} \tag{12}$$

Replacing ΔS_{conf} with $\Delta\Delta S_{conf}$ yields an expression for ΔN_{fold}, the difference in the number of residues involved in the ligation-associated conformational changes for two proteins:

$$\Delta N_{fold} = \frac{\Delta\Delta S_{conf}}{-5.6} \tag{13}$$

In the present case, ΔN_{fold} for α 49–50 and wild-type α-PV would equal $-68/-5.6$, or 12 residues, roughly 11% of the protein. This analysis suggests that the combined I49F and L50I mutations produce a conformation of the apo-protein that undergoes substantial folding when Ca^{2+} binds.

Whereas wild-type rat α-PV unfolds at 45.2 °C, in PBS containing EDTA, α 49–50 exhibits a T_m of 32.9, with a denaturational ΔH_{vH} of 51.0 kcal mol^{-1} (Fig. 7A and Table 4). Thus, the combined I49F and L50I mutations seriously destabilize the protein. The ratio of ΔH_{vH}: ΔH_{cal} is approximately 1.0, indicating that the α 49–50 variant unfolds via a two-state transition, with negligible population of partially unfolded states. Evidently, the folding that accompanies Ca^{2+} binding reflects the transition between fully unfolded and native forms of the protein.

At a given temperature T, the fraction of unfolded protein, $\alpha(T)$, is equal to

$$\alpha(T) = \frac{K(T)}{1 + K(T)} \tag{14}$$

where $K(T)$ is the equilibrium constant for unfolding. At the T_m, the equilibrium constant, $K(T_m)$, is equal to 1.0. Thus, the equilibrium constant at 298 K is given by

$$K(298) = \exp\left[\frac{-\Delta H_{vH}}{R}\left(\frac{1}{298} - \frac{1}{T_m}\right)\right] \tag{15}$$

Over a limited temperature-range, neglecting the temperature-dependence of ΔH_{vH} does not introduce a serious error. Substituting the observed values for T_m and ΔH_{vH} – i.e., 306 K and 51.0 kcal mol^{-1} – yields a value of 0.10 for $K(298)$. Thus, the fraction of unfolded protein at 298 K is approximately 0.10/1.10, or 0.09. This estimate – that roughly 9% of the protein is unfolded at the 25 °C – agrees reasonably well with the one obtained by analysis of the entropy-changes accompanying Ca^{2+} binding. It also provides a straightforward explanation for the heightened exothermicity associated with the EF-site binding event. Specifically, the EF-site binding enthalpy is more exothermic than the CD-site enthalpy in α 49–50 because binding of the first metal ion (at the EF site) is accompanied by the refolding of a portion of the ensemble. By contrast, the second ion binds to a folded population of molecules, so that the binding enthalpy reflects the intrinsic value.

In Ca^{2+}-free rat β-PV, the side-chains of F49, I50, and L85 associate noncovalently in dovetail fashion in the protein interior (Fig. 11A). When Ca^{2+} binds, this interaction is abolished (Fig. 11B). In wild-type rat α-PV, the 49-50-85 interaction is not observed in the Ca^{2+}-free protein. Instead, the residues occupy positions similar to those observed in the Ca^{2+}-bound form (Fig. 11C, D). The α 49–50 variant includes the triad of residues – F49, I50, and L85 – that produces the dovetail arrangement observed in the structure of Ca^{2+}-free rat β. However, the preceding analyses strongly suggest that apo- α 49–50 does not adopt a similar configuration and that, in fact, the introduction of F49 and I50 seriously destabilizes the rat α-PV molecule, presumably by disrupting the hydrophobic core.

3.8. The α 49–58 variant

Although introduction of I58L mutation into α 49–57 produces only a modest change in Ca^{2+} affinity ($\Delta\Delta G_{total} = +0.17$ kcal mol^{-1}), the mutation strongly perturbs the Ca^{2+}-binding enthalpy – raising $\Delta H_{Ca,total}$ from -11.12 to -7.86 kcal mol^{-1} at 25 °C. The magnitude of the overall ΔC_p associated with Ca^{2+} binding to α 49–58 is substantially reduced relative to α 49–50, from -0.20 to -0.082 kcal mol^{-1} K^{-1} (Table 3). Substituting the corresponding $\Delta\Delta C_p$ of -0.07 kcal K^{-1} mol^{-1}, relative to wild-type α, into Eq. (11) returns an estimate for $\Delta\Delta S_{solv}$ of 18 cal K^{-1} mol, and $\Delta\Delta S_{bind}$ is -8.0 cal K^{-1} mol^{-1} (Table 2). Supplied with these values, Eq. (9) yields a value for $\Delta\Delta S_{conf}$ of -26 cal K^{-1} mol^{-1}, which corresponds to a ΔN_{fold} value of 4.6. Thus, approximately 4% of the α 49–58 variant undergoes ligation-promoted folding – substantially lower than the 11% obtained in the preceding analysis of α 49–50.

This result implies that swapping leucine for I58 stabilizes the α 49–50 variant, a conclusion supported by DSC measurements. The T_m of α 49–58 (36.8 °C) is a full 3.9 degrees higher than that of α 49–50. Substitution of this T_m value and the observed denaturational enthalpy (53.8 kcal mol^{-1}) into Eq. (15) yields an estimate for the equilibrium constant at 298 K of 0.032. The predicted fraction of unfolded protein at 25 °C would then be 0.031, corresponding to about 3.4 residues, in good agreement with the entropy-based estimate above. Thus, both binding- and stability data for the α 49–58 variant indicate that replacing the I58 at position 58 with leucine permits the hydrophobic core of the Ca^{2+}-free protein to accommodate the side-chains of F49 and I50 with less disruption.

In the Ca^{2+}-bound state, paired EF-hand motifs invariably display a one-residue segment of antiparallel β-structure, formed by the amide moieties of the residues residing at position 8 in each binding loop. Whereas this β-fragment persists in the Ca^{2+}-free structure of rat α-PV, it is not observed in the apo-form of rat β-PV. In the α isoform,

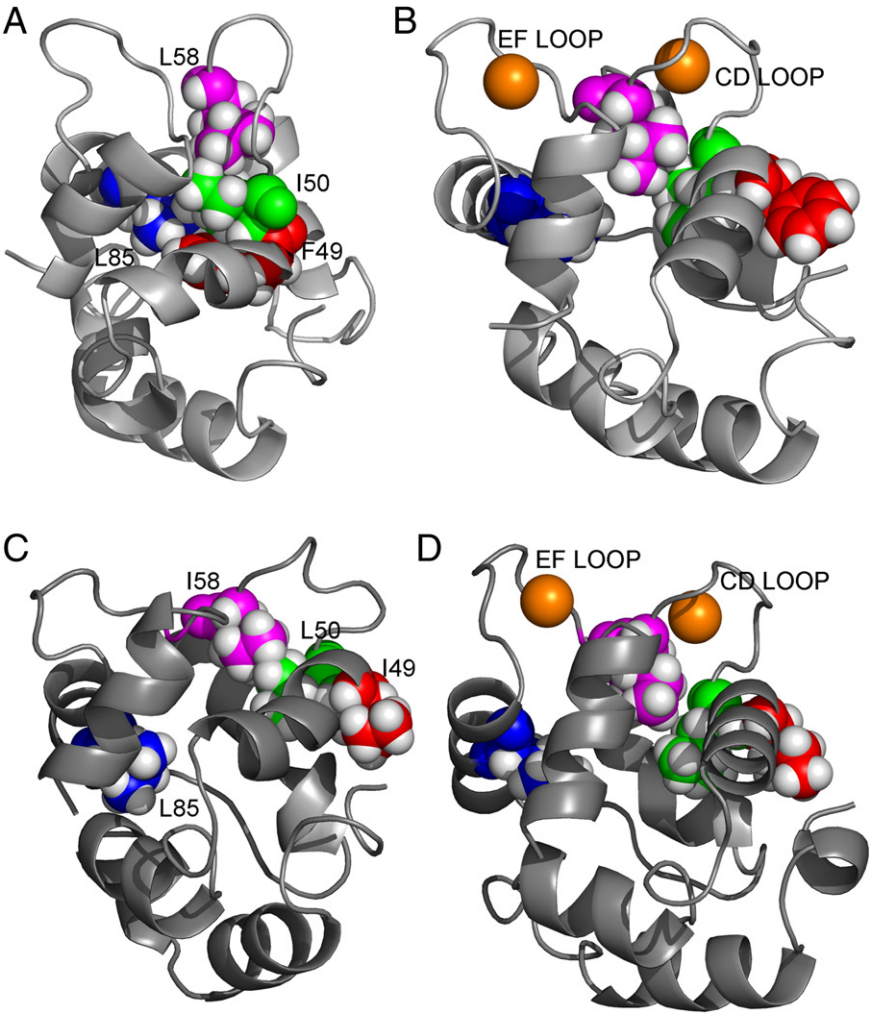

Fig. 11. Orientation of residues 49, 50, and 85 in rat α- and β-parvalbumins. Heavy atoms in residues 49, 50, and 85 are rendered in red, green, and blue, respectively. Residue 58 is also displayed (magenta) to suggest how it might influence the orientations of the other three residues. (A) Ca^{2+}-free rat β-PV (PDB 2NLN). (B) Ca^{2+}-bound rat β-PV (PDB 1RRO). (C) Ca^{2+}-free rat α-PV (PDB 2JWW). (D) Ca^{2+}-bound rat α-PV (PDB 1RWY).

isoleucine is present at position 8 in both the CD and EF loops (residues 58 and 97, respectively). It has been suggested [29] that steric strain between I58 and I97 could produce a conformation of the binding loops conducive to formation of the β-fragment. If correct, then replacement of I58 by leucine might eliminate the steric strain, allowing the residues in the binding loop to adopt a conformation more compatible with the presence of F49 and I50.

NMR dynamics studies on the α 49–50 and α 49–58 variants might furnish additional insight into the impact of the L50I and I58L mutations on α-PV protein stability. There is an emerging consensus that side-chain methyl dynamics can serve as a meaningful indicator of conformational entropy [30–33]. That viewpoint assumes that methyl-bearing side-chains are sufficiently well-coupled to adjacent side-chains to report on their motions and sufficiently well-distributed to provide a molecule-wide representation depiction of side-chain motion. Assuming that complications of exchange-broadening could be avoided – e.g., by collecting data at low temperature – side-chain-dynamics studies on the α-PV variants could potentially reveal whether the L50I and I58L mutations exert their impact locally or throughout the molecule. We have previously examined the backbone-dynamics of the high-affinity variants of rat β-parvalbumin, S55D and G98D [34]. Although both mutations similarly improve the Ca^{2+} affinity of the local binding sites – CD and EF, respectively – only the S55D mutation provoked a general increase in backbone motions with correlation times exceeding 20 ps.

3.9. The α 49–59 variant

When the E59D mutation is introduced into α 49–58, the total binding enthalpy becomes still less exothermic, rising from −7.86 to −6.62 kcal mol^{-1}, and the accompanying change in heat capacity (Table 3) shrinks further in magnitude and actually changes sign ($\Delta C_p = 0.02$). The implication is that, continuing the trend begun by the Y57F and I58L mutations, introduction of E59D further reverses the destabilization provoked by F49 and I50. This suggestion is again supported by DSC measurements. Whereas α 49–58 unfolds at 36.8 °C, the α 49–59 variant exhibits a T_m of 39.4 °C.

It would appear that the side-chains of F49 and I50, in isolation, are not well-tolerated by the wild-type rat α-PV tertiary structure – with two lines of reasoning indicating that the resulting apo-protein is partially unfolded at 25 °C. However, the introduction of L58 and D59 evidently allows the protein to adopt a more compact conformation – presumably by facilitating more effective packing of F49 and I50 in the hydrophobic core. It would be interesting to determine to what degree, if any, the conformation of Ca^{2+}-free α 49–59 resembles that of Ca^{2+}-free rat β.

3.10. The L85F variants

With the replacement of L85 by phenylalanine, Ca^{2+} binding becomes substantially more exothermic in several of the CD-loop variants. For example, although the L85 mutation has no impact on the Ca^{2+}

affinity of α 49–50, the total enthalpy change at 25 °C associated with Ca^{2+} binding falls from −11.19 to −15.53 kcal mol^{-1}. The overall ΔC_p value, −0.34 kcal K^{-1} mol^{-1}, is also substantially larger than that of α 49–50. Application of Eqs. (2)–(7) ultimately yields a value for ΔN_{fold} value of 21. Relative to wild-type α, approximately 20% more of the α 49–50/85 variant undergoes ligation-promoted folding. Apparently, L85F further destabilizes α 49–50.

That conclusion is supported by DSC data for α 49–50/85. The observed T_m is 31.6 °C (304.8 K), 1.3 degrees lower than that of α 49–50, and the van't Hoff enthalpy for denaturation is 43.8 kcal mol^{-1}. Substitution of these values into Eq. (15) yields an estimate for the equilibrium constant for unfolding, at 298 K, of 0.19. The calculated fraction unfolded is thus 0.16, which corresponds to approximately 18 residues, in reasonable agreement with the estimate derived from the entropy-based calculation.

L85F does not produce a major increase in exothermicity in all of the α CD-loop variants. As shown in Fig. 9B, substantial $\Delta\Delta H_{Ca}$ values (in kcal mol^{-1}) are observed for I49F (−1.99), 49–50 (−4.34), 49–57(−4.25), 49–58 (−2.15), and 49–60 (−2.56). Interestingly, however, E59D appears to suppress the impact of L85F on ΔH – i.e., the magnitudes of $\Delta\Delta H_{Ca}$ are substantially smaller in 49–59 (−0.56), E59D (−0.58), and 59–60 (−0.74). This attenuating effect of E59D is reminiscent of its impact in α 49–58, further supporting the notion of communication between the hydrophobic core and residue 59.

There is clearly precedent for residues outside the metal-ion-binding pockets exerting long-range influence on metal-ion-binding behavior. In calmodulin (CaM), for example, the N- and C-terminal domains are joined by a flexible linker (residues 76–81). The Ca^{2+} affinity of the N-domain is depressed in the intact protein, relative to that of the isolated N-domain – evidence for a negatively cooperative inter-domain interaction transmitted by the flexible linker. Consistent with this idea, Ca^{2+} binding in the C-domain indirectly stabilizes the linker sequence. It is now generally accepted that the linker functions as a Ca^{2+}-regulated conformational switch [35,36].

One of the reviewers of this manuscript astutely observed that L85 occupies a position in the parvalbumin CD-EF domain analogous to that of M51 in calmodulin. M51 contributes to the "FLMM pocket" in the N-terminal CaM-domain, along with F19, L32, and M71. These FLMM tetrads – there is a corresponding one in the C-terminal domain as well – evidently secure an anchor-residue in CaM target-peptides [37,38]. The reviewer suggested that, by analogy to CaM, L85 might influence the association between the CD-EF domain and the AB domain – pointing out that F30 resembles an anchor-residue in CaM targets. In fact, L85 does contact both F30 and F24 in the Ca^{2+}-bound structures of the α- and β-PV isoforms.

If L85 corresponds to M51 in CaM, then residues 66 and 105 in the parvalbumin sequence reside at positions corresponding to CaM residues L32 and M71. These two residues bracket L85 in the hydrophobic core of the Ca^{2+}-bound protein – I66 and L105 in the α-PV, F66 and M105 in the β isoform. The analogy to the CaM system is not perfect. The residue corresponding to CaM F19 is D53, a coordinating residue, in the parvalbumin primary structure. However, it may be significant that residues 66, 85, and 105 form an FLM triad in the β-PV sequence, whereas they form an ILL triad in the α isoform. Perhaps the residues bracketing L85 in the β system allow for greater conformational malleability.

4. Concluding remarks

The results of this study raise several questions. Why does E-D exchange at residue 59 have a much greater impact in the rat α isoform? Why are the perturbations of divalent-ion affinity resulting from the CD-loop mutations confined to the CD site? Why are the F49, L50, and F85 mutations so destabilizing?

Some years ago, we examined the Ca^{2+}-binding behavior of the noncovalent complexes formed between the AB and CD-EF domains from rat α- and β-PV [39]. Not surprisingly, the α AB/CD-EF complex exhibited the superior affinity, $\Delta G_{tot} = -16.1$ kcal mol^{-1} vs. -12.7 kcal mol^{-1} for the β isoform. We also studied the heterologous complexes. Whereas the β AB/α CD-EF complex displayed markedly diminished Ca^{2+} affinity compared to the α/α complex (−12.5 vs. -16.1 kcal mol^{-1}), the Ca^{2+}-affinity of the α AB/β CD-EF greatly surpassed that of the homologous β/β complex (−15.0 vs −12.7 kcal mol^{-1}). Moreover, although the sequences of the α and β AB domains differ at 18 of 37 positions, in the presence of saturating Ca^{2+}, the apparent association constant measured for α/β complex formation was more than twice the value measured for β/β (6.6×10^6 vs. 3.0×10^6 M^{-1}). These findings strongly suggested that the side-chains contributed by the AB domain to the hydrophobic core influence the divalent ion-binding properties of the CD-EF domain. Conceivably, then, the disparate consequences of the CD-loop mutations and L85F in rat α- and β-PV could reflect differing interactions between the AB and CD-EF domains in the two proteins. The biological function of the mammalian β isoform (presently uncertain) is presumably contingent on its low-affinity divalent-ion-binding signature and, more specifically, the Ca^{2+}-specific behavior of the CD site. If restoration of a Ca^{2+}/Mg^{2+} phenotype would have adverse physiological consequences, the sequence may have evolved to insure that the single mutation of D59 to glutamate would not seriously perturb divalent ion-binding. Thus, the non-canonical substitutions in the CD-loop, residue 85, and in the AB domain might serve to lock the apo-protein into a conformation energetically distinct from the Ca^{2+}-bound one.

It is curious, then, that the rat α sequence is not similarly insulated from the consequences of E-D exchange at residue 59. By sequestering Ca^{2+}, the α isoform facilitates relaxation of skeletal myofibrils and rapidly-firing neurons. Transformation of the high-affinity CD site in rat α to a Ca^{2+}-specific one, via E59D, would undoubtedly compromise this activity. However, the EF-site would still retain its Ca^{2+}/Mg^{2+} character in the mutated protein. Conceivably, compensation for the loss of buffering-capacity, attendant to mutation of the CD site, could be achieved simply by increased expression.

Acknowledgment

The authors acknowledge financial support from the Department of Biochemistry at the University of Missouri, the University of Missouri Research Board, and National Science Foundation (MCB0543476).

References

[1] R.H. Kretsinger, Structure and evolution of calcium-modulated proteins, CRC Crit. Rev. Biochem. 8 (1980) 119–174.
[2] H. Kawasaki, R.H. Kretsinger, Calcium-binding proteins 1: EF-hands, Protein Profile 2 (1995) 297–490.
[3] M.R. Celio, T. Pauls, B. Schwaller, Guidebook to the calcium-binding proteins, Oxford University Press, New York, 1996.
[4] J.L. Gifford, M.P. Walsh, H.J. Vogel, Structures and metal-ion-binding properties of the Ca^{2+}-binding helix-loop-helix EF-hand motifs, Biochem. J. 405 (2007) 199–221.
[5] R.H. Kretsinger, C.E. Nockolds, Carp muscle calcium-binding protein. II. Structure determination and general description, J. Biol. Chem. 248 (1973) 3313–3326.
[6] T.L. Pauls, J.A. Cox, M.W. Berchtold, The Ca^{2+}-binding proteins parvalbumin and oncomodulin and their genes: new structural and functional findings, Biochim. Biophys. Acta 1306 (1996) 39–54.
[7] S.H. Arif, A Ca^{2+}-binding protein with numerous roles and uses: parvalbumin in molecular biology and physiology, BioEssays 31 (2009) 410–421.
[8] B. Schwaller, The continuing disappearance of "pure" Ca^{2+} buffers, Cell. Mol. Life Sci. 66 (2009) 275–300.
[9] U.G. Fohr, B.R. Weber, M. Müntener, W. Staudenmann, G.J. Hughes, S. Frutiger, D. Banville, B.W. Schafer, C.W. Heizmann, Human α and β parvalbumins. Structure and tissue-specific expression, Eur. J. Biochem. 215 (1993) 719–727.
[10] N. Sakaguchi, M.T. Henzl, I. Thalmann, R. Thalmann, B.A. Schulte, Oncomodulin is expressed exclusively by outer hair cells in the organ of Corti, J. Histochem. Cytochem. 46 (1998) 29–39.
[11] Y. Yin, M.T. Henzl, B. Lorber, T. Nakazawa, T.T. Thomas, F. Jiang, R. Langer, L.I. Benowitz, Oncomodulin is a macrophage-derived signal for axon regeneration in retinal ganglion cells, Nat. Neurosci. 9 (2006) 843–852.

[12] M.T. Henzl, J.D. Larson, S. Agah, Influence of monovalent cation identity on parvalbumin divalent ion-binding properties, Biochemistry 43 (2004) 2747–2763.
[13] C.A. Bottoms, J.P. Schuermann, S. Agah, M.T. Henzl, J.J. Tanner, Crystal structure of rat α-parvalbumin at 1.05 Å resolution, Protein Sci. 13 (2004) 1724–1734.
[14] M.T. Henzl, J.J. Tanner, Solution structure of Ca^{2+}-free rat β-parvalbumin (oncomodulin), Protein Sci. 16 (2007) 1914–1926.
[15] M.T. Henzl, K. Ndubuka, Low-affinity signature of the rat β-parvalbumin CD site. Evidence for remote determinants, Biochemistry 46 (2007) 23–35.
[16] M.T. Henzl, M.E. Davis, A. Tan, Leucine-85 is an important determinant of divalent Ion affinity in rat β-parvalbumin (oncomodulin), Biochemistry 47 (2009) 13635–13646.
[17] M.T. Henzl, J.S. Graham, Conformational stabilities of the rat α- and β-parvalbumins, FEBS Lett. 442 (1999) 241–245.
[18] R.C. Hapak, P.J. Lammers, W.A. Palmisano, E.R. Birnbaum, M.T. Henzl, Site-specific substitution of glutamate for aspartate at position 59 of rat oncomodulin, J. Biol. Chem. 264 (1989) 18751–18760.
[19] M. Haner, M.T. Henzl, B. Raissouni, E.R. Birnbaum, Synthesis of a new chelating gel: removal of Ca^{2+} ions from parvalbumin, Anal. Biochem. 138 (1984) 229–234.
[20] M.T. Henzl, Characterization of parvalbumin and polcalcin divalent ion binding by isothermal titration calorimetry, Methods Enzymol. 455 (2009) 259–296.
[21] M.T. Henzl, L.A. Markus, M.E. Davis, A.T. McMillan, Simultaneous addition of two ligands: a potential strategy for estimating divalent ion affinities in EF-hand proteins by isothermal titration calorimetry, Methods 59 (2013) 336–348.
[22] M.T. Henzl, J.D. Larson, S. Agah, Estimation of parvalbumin Ca^{2+}- and Mg^{2+}-binding constants by global least-squares analysis of isothermal titration calorimetry data, Anal. Biochem. 319 (2003) 216–233.
[23] M.T. Henzl, S. Agah, J.D. Larson, Rat α- and β-parvalbumins: Comparison of their pentacarboxylate and site-interconversion variants, Biochemistry 43 (2004) 9307–9319.
[24] M.T. Henzl, J.D. Larson, S. Agah, Influence of monovalent cations on rat α- and β-parvalbumin stabilities, Biochemistry 39 (2000) 5859–5867.
[25] J.A. Cox, M. Milos, J.P. MacManus, Calcium- and magnesium-binding properties of oncomodulin. Direct binding studies and microcalorimetry, J. Biol. Chem. 265 (1990) 6633–6637.
[26] R.L. Baldwin, Temperature dependence of the hydrophobic interaction in protein folding, Proc. Natl. Acad. Sci. U. S. A. 83 (1986) 8069–8072.
[27] K.P. Murphy, P.L. Privalov, S.J. Gill, Common features of protein unfolding and dissolution of hydrophobic compounds, Science 247 (1990) 559–561.
[28] R.S. Spolar, M.T. Record Jr., Coupling of local folding to site-specific binding of proteins to DNA, Science 263 (1994) 777–784.
[29] R.R. Biekofsky, S.R. Martin, J.P. Browne, P.M. Bayley, J. Feeney, Ca^{2+} coordination to backbone carbonyl oxygen atoms in calmodulin and other EF-hand proteins: ^{15}N chemical shifts as probes for monitoring individual-site Ca^{2+} coordination, Biochemistry 37 (1998) 7617–7629.
[30] M.S. Marlow, J. Dogan, K.K. Frederick, K.G. Valentine, A.J. Wand, The role of conformational entropy in molecular recognition by calmodulin, Nat. Chem. Biol. 6 (2010) 352–358.
[31] S.-R. Tzeng, C.G. Kalodimos, Protein activity regulation by conformational entropy, Nature 488 (2012) 236–240.
[32] V. Kasinath, K.A. Sharp, A.J. Wand, Microscopic insights into the NMR relaxation-based protein conformational entropy meter, J. Am. Chem. Soc. 135 (2013) 15092–15100.
[33] A.J. Wand, The dark energy of proteins comes to light: conformational entropy and its role in protein function revealed by NMR relaxation, Curr. Opin. Struct. Biol. 23 (2013) 75–81.
[34] M.T. Henzl, W.G. Wycoff, J.D. Larson, J.J. Likos, ^{15}N nuclear magnetic resonance relaxation studies on rat β-parvalbumin and the pentacarboxylate variants, S55D and G98D, Protein Sci. 11 (2002) 158–173.
[35] Z. Qin, T.C. Squier, Calcium-dependent stabilization of the central sequence between Met^{76} and Ser^{81} in vertebrate calmodulin, Biophys. J. 81 (2001) 2908–2918.
[36] O.R. Jaren, J.K. Kranz, B.R. Sorensen, A.J. Wand, M.A. Shea, Calcium-induced conformational switching of *Paramecium* calmodulin provides evidence for domain coupling, Biochemistry 41 (2002) 14158–14166.
[37] Z.A. Ataman, L. Gakhar, B.R. Sorensen, J.W. Hell, M.A. Shea, The NMDA receptor NR1 C1 region bound to calmodulin: structural insights into functional differences between homologous domains, Structure 15 (2007) 1603–1617.
[38] H. Ishida, H.J. Vogel, Protein-peptide interactions studies demonstrate the versatility of calmodulin target protein binding, Protein Pept. Lett. 13 (2006) 455–465.
[39] M.T. Henzl, S. Agah, J.D. Larson, Association of the AB and CD-EF domains from rat α- and β-parvalbumin, Biochemistry 43 (2004) 10906–10917.